Kidneys

12

S. Ted Treves, Alan B. Packard,
and Frederick D. Grant

Nuclear medicine techniques play a very important role in the initial diagnosis and follow-up of many renal diseases in children. These techniques are physiological, minimally invasive, and highly sensitive. They enable early detection of renal disease, even before structural changes become apparent on anatomic imaging. Nuclear medicine provides unique functional and anatomic information with minimal risk to the patient. Radionuclide techniques can be used safely in all pediatric age groups and in severely ill patients, including those with renal insufficiency or other renal impairment. These techniques require only a very small amount of tracer material (0.02–0.08 mg) in a very small volume of solution delivered by intravenous injection (0.1–0.5 mL). Radiopharmaceuticals administered in renal studies do not produce pharmacologic, osmotic, hemodynamic, or toxic effects. Renal radiotracers can be administered safely even in patients allergic to iodinated contrast agents. The radiation exposures to the patients are very low. Indications for these studies in children are listed in Table 12.1. For the vast majority of pediatric patients, sedation is not required for these studies. If motion occurs, motion correction techniques can be applied effectively [1].

The extensive use of ultrasonography has provided a clear indication of the incidence of renal disease during the prenatal and neonatal periods [2]. The complementary nature of nuclear medicine and other diagnostic imaging methods for the pediatric urinary tract, especially ultrasonography, should be emphasized. In many instances, a combined approach allows the determination of anatomic-functional relationships, which often provide additional insight into the nature and severity of the problem under investigation.

S.T. Treves, MD
Joint Program in Nuclear Medicine,
Department of Radiology, Harvard Medical School,
Boston, MA, USA

Division of Nuclear Medicine and Molecular Imaging,
Department of Radiology, Boston Children's Hospital,
Boston, MA, USA

Division of Nuclear Medicine and Molecular Imaging,
Department of Radiology,
Brigham and Women's Hospital,
Boston, MA, USA
e-mail: ted_treves@hms.harvard.edu

A.B. Packard
Joint Program in Nuclear Medicine,
Department of Radiology, Harvard Medical School,
Boston, MA, USA

Division of Nuclear Medicine and Molecular Imaging,
Department of Radiology,
Boston Children's Hospital,
Boston, MA, USA
e-mail: alan.packard@childrens.harvard.edu

F.D. Grant
Joint Program in Nuclear Medicine,
Department of Radiology, Harvard Medical School,
Boston, MA, USA

Division of Nuclear Medicine and Molecular Imaging,
Department of Radiology,
Boston Children's Hospital,
Boston, MA, USA

Department of Radiology,
Brigham and Women's Hospital, Boston, MA, USA
e-mail: frederick.grant@childrens.harvard.edu

S.T. Treves (ed.), *Pediatric Nuclear Medicine and Molecular Imaging*,
DOI 10.1007/978-1-4614-9551-2_12, © Springer Science+Business Media New York 2014

Table 12.1 Indications of nuclear medicine renal studies in children

Hydronephrosis and obstruction
Pre- and post-surgery/interventions
Pyelonephritis
Vesicoureteral reflux
Renal function. Split renal function
Cortical integrity. Scarring
Hypertension
Duplication
MCDK
Ectopia, cross fused renal ectopia
Congenital anomalies. Horseshoe kidney
Renal transplants
Urinary leak
Trauma
GFR

Collectively, congenital abnormalities account for approximately 42 % of cases of chronic renal failure [3]. The incidence of end-stage renal disease in children in the USA is approximately 11 new cases per one million total population per year [4]. Koenigsberg et al. reported that the incidence of preexisting lesions is 15–23 % in children showing serious renal injury following relatively minor trauma [5]. Associated anomalies of other organs are not uncommon. For example, infections of the urinary tract affect 3–5 % of all children. During the neonatal period, male infants are more commonly affected, but after 3 months of age, female children are affected approximately three times more often than males [6]. Approximately 10 % of the population is affected by renal anomalies, but many of these problems are minor and of no clinical significance. Excluding polycystic kidneys, the incidence of major malformations has been estimated at 4–7 per 1,000 [7]. A screening study using ultrasonography on more than 132,000 school children of both sexes revealed renal abnormalities in approximately 0.5 % of the subjects [8]. Early diagnosis and treatment of abnormalities of the urinary tract in children can reduce morbidity and mortality [9]. The high-sensitivity, noninvasive, and physiologic nature of diagnostic nuclear medicine places it in a central role in the diagnosis of renal disorders and the evaluation of renal function in pediatric patients. This chapter will review dynamic and static renal scintigraphy and its clinical applications.

Radiopharmaceuticals used in the evaluation of the kidneys may be classified into two groups. The first group includes radiopharmaceuticals that are rapidly eliminated by the kidneys and thus enable evaluation of both renal function and urine drainage. This group includes ^{99m}Tc-mercaptoacetyltriglycine (^{99m}Tc-MAG3) and ^{99m}Tc-diethylenetriaminepentaacetic acid (^{99m}Tc-DTPA), as well as ^{99m}Tc-glucoheptonate and ^{123}I-orthoiodohippurate (^{123}I-OIH).

The second group includes radiopharmaceuticals that concentrate in the renal parenchyma for a sufficiently long period so that detailed scintigraphic mapping of regional functioning renal parenchyma is possible. The current agent of choice for static renal cortical imaging is ^{99m}Tc-dimercaptosuccinic acid (^{99m}Tc-DMSA). Selection of the renal agent depends largely on the diagnostic problem to be investigated and on the practitioner's experience and preference. In general, it is best to become familiar with one agent for dynamic renal scintigraphy and one for static renal scintigraphy and to use them consistently. Many pediatric patients affected with renal disease require follow-up evaluations, and the use of the same radiopharmaceutical and technique facilitates assessment of change.

Dynamic Renal Scintigraphy

Procedure

Whenever possible, it can be useful to provide the patient and the caregiver(s) detailed explanations about the procedure in advance so that they know what to expect when they arrive in the nuclear medicine department. Parents may have questions and concerns about the need for an intravenous injection, bladder catheterization, study duration, radiation exposure, and other

risks. Information brochures can be given to the patient by the referring physician's office. Additionally, such information brochures can be placed on an appropriate website for easy access by the patient and families. The nuclear medicine physician reviews the indications for the study and determines if there are any special procedural considerations or if the use of a diuretic should be anticipated. Upon arrival to the department, the patient is greeted by a nuclear medicine technologist or a child life specialist who will review the procedure further and answer any questions. Recent administration of intravenous contrast agents may affect the renogram by reducing renal uptake or clearance of radiopharmaceutical for up to 24 h. Therefore, dynamic radionuclide studies of the kidneys should be performed either before or 24 h after the administration of radiographic contrast agents.

Patients should be encouraged to drink fluids approximately 1 h prior to the study. In pediatric practice, however, it is difficult to implement a standard pre-study hydration method; therefore, many children end up being examined in their normal state of hydration. When possible, patients are encouraged to empty their bladder before the examination begins. A catheter should be inserted into the bladder if the patient cannot or will not void. The bladder should be allowed to drain through the catheter during the entire duration of the study. Intravenous access is established using a butterfly needle (23–25 gauge) or a short intravenous catheter that is securely fastened to the skin with tape. Before proceeding, one must ensure that intravenous access is reliable and stable. Next, an intravenous infusion of normal saline (10–15 mL/kg) is begun and should be maintained during the first 20 min of the study and continued as necessary to include diuretic renography when this is indicated. Extravasation of the tracer can ruin the examination and must be avoided at by ensuring patency of the intravenous access. Partial extravasation can severely compromise the quality of the study and, if not recognized, may yield to erroneous interpretation.

Radiopharmaceuticals and Administered Doses

^{99m}Tc-MAG3

Technetium-99m-MAG3 (Mallinckrodt, St Louis, MO) is the current agent of choice for dynamic renal scintigraphy [10–15]. The agent is excreted principally through active renal tubular transport. Because ^{99m}Tc-MAG3 is eliminated by tubular secretion and has a high initial renal uptake, it produces high kidney/background ratios, which provide good images of the renal cortex. Its rapid excretion provides good temporal resolution. The usual administered dose of ^{99m}Tc-MAG3 for radionuclide angiography is 5.55 MBq/kg of body weight (0.15 mCi/kg) with a minimum of 37 MBq (1.0 mCi) and a maximum of 148 MBq (4.0 mCi). When radionuclide angiography is not needed, the usual dose of this agent is lower: 3.7 MBq/kg (0.1 mCi/kg) with a minimum of 37 MBq (1.0 mCi) and a maximum of 148 MBq (4 mCi) [16].

The use of noise reduction software may facilitate even further reductions in the administered dose [17].

^{99m}Tc-DTPA

Technetium-99m-DTPA has been used for dynamic renal scintigraphy for several decades, but largely has been replaced by ^{99m}Tc-MAG3. Technetium-99m-DTPA is excreted primarily by glomerular filtration, although with a lower renal clearance rate than ^{99m}Tc-MAG3 [18–29]. A lower rate of glomerular filtration compared with inulin is probably due to protein binding, the amount of which varies with the formulation [30]. A maximum concentration of 5 % in each kidney is achieved 2–3 min after injection [31].

^{99m}Tc-Glucoheptonate

Technetium-99m-glucoheptonate is promptly taken up by the kidneys and rapidly eliminated in the urine. By 1 h after injection, 8–10 % of the initial tracer activity is present in the kidneys and almost 40 % of the administered dose has been eliminated in the urine [32]. Therefore, this

radiopharmaceutical offers the opportunity for both a dynamic renogram and renal cortical scintigraphy, but this rarely is done [33].

^{123}I-Orthoiodohippurate (OIH)

Iodine-123-OIH is useful for dynamic renal scintigraphy because of its high uptake by the renal tubules and rapid excretion into the urine. Iodine-123-OIH has been used extensively in Europe, but the use of this agent in the USA has been limited. This radiopharmaceutical is excreted by the kidneys similarly to para-aminohippuric acid (PAH), the standard for the measurement of effective renal plasma flow [34]. Approximately 80 % of PAH is eliminated by tubular secretion and 20 % by glomerular filtration, with an extraction ratio of approximately 0.9 [35], which is approximately 85 % that of PAH [36].

The Renogram: Procedure

Dynamic renal scintigraphy or renogram consists of serial imaging following the intravenous injection of the radiotracer. Dynamic renal scintigraphy can include three phases: (1) radionuclide angiography, (2) dynamic renal scintigraphy, and (3) diuretic renography. The diuretic of choice for diuretic renography is the loop diuretic furosemide. There are three approaches to the administration of furosemide for diuretic renography. In North America, most practitioners administer furosemide after the completion of the initial 20-min dynamic renal study, usually within 30 min after the administration of ^{99m}Tc-MAG3. This has been referred as the F+20 diuretic renogram. Another approach is to administer furosemide simultaneously with ^{99m}Tc-MAG3 (F-0). This shortens overall imaging time, but results in diuretic administration to all patients. A third approach is to administer diuretic approximately 15 minutes (F-15) before administration of ^{99m}Tc-MAG3.

Children typically are examined in the supine position with the gamma camera placed underneath the examining table, viewing the area of the kidneys and bladder. In the supine position, the distance from the skin to each of the kidneys is approximately the same, and for the calculation of the left-to-right renal uptake ratio, depth correction is not done. Recipients of renal transplants located in the pelvis are examined in the supine position with the gamma camera viewing the kidney and the bladder from the anterior projection. Appropriate immobilization equipment should be employed to reduce patient motion. Sedation for this test is used very exceptionally, if ever. The gamma camera is equipped with a parallel-hole, low-energy, high-resolution collimator. Electronic magnification is employed according to the patient's size. After the patient is positioned, the tracer is administrered as a rapid intravenous bolus injection, and recording of the study is begun simultaneously with the injection.

Imaging: Radionuclide Angiography

Radionuclide angiography consists of rapid imaging of the initial minute of the renogram following the rapid intravenous injection of the tracer. Radionuclide angiography is almost never used alone and it is typically recorded during the first minute of a dynamic renogram. If the study includes a radionuclide angiogram, recording is begun at 0.25 s per frame for 60 s, immediately followed by dynamic renal scintigraphy. As few pediatric renograms are performed to evaluate the vascular supply to the kidney, images from the angiographic phase of the renogram are rarely acquired in children. The high frame rate needed for angiography requires administration of higher doses of ^{99m}Tc-MAG3. Therefore, radiation exposure can be decreased by eliminating this phase of the renogram. However, for special indications, such as evaluation of possible aortic or renal artery stenosis, the angiographic phase may be a useful part of the renogram. In practice, however, most of the relevant information about renal perfusion can be obtained from the 20-min dynamic scintigraphy phase.

Imaging: Dynamic Renal Scintigraphy

The dynamic phase of the renogram is acquired at a slower frame rate than the angiographic

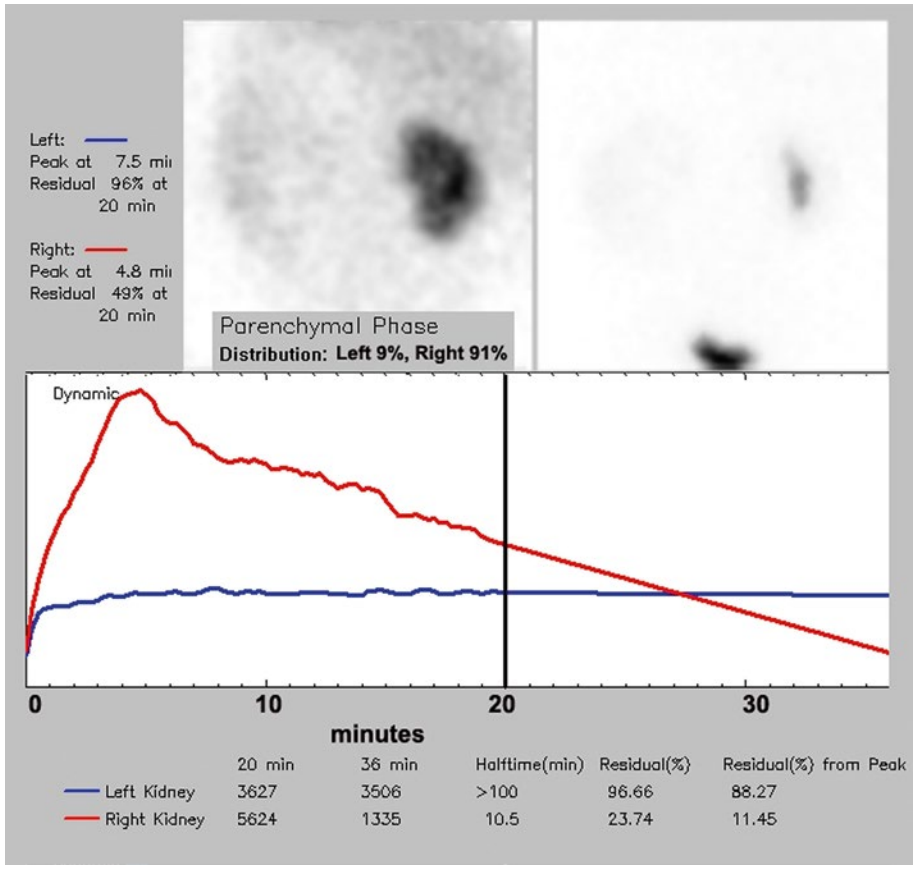

Fig. 12.1 Dynamic renography in a 4-month-old male with left multicystic dysplastic kidney and with grade 3 vesicoureteral reflux into the right kidney. Differential function is 9 % left kindey and 91 % right kidney as assessed during the second minute of imaging (*top left panel*). After twenty minutes (*top right panel*), the dysplastic left kidney shows no tracer uptake. The right kidney has 49% residual tracer in the collecting system. After postural drainage (*bottom panel*), a repeat image at 36 minutes demonstrates additional collecting system drainage with a residual of 11% of peak activity

phase. For our protocol, images are acquired at 15 seconds per frame for twenty minutes (128 x 128 matrix). At the end of the 20-min renogram, the nuclear medicine physician reviews the study and determines if there is enough information to answer the diagnostic question or if additional images and/or a diuretic renogram is needed.

If there is spontaneous, but slow, drainage of tracer, the patient can be instructed to get up (if possible), void in the bathroom, and walk around for a few minutes in order to promote postural drainage before another image of the kidneys is obtained. In a small child or a baby, the patient should be picked up and held by a caregiver for a few minutes before taking additional images (Fig. 12.1). If adequate postural drainage is not seen, the nuclear medicine physician may decide to proceed with a diuretic renogram. If postural drainage occurs, then administration of furosemide may not be necessary.

Imaging: MRI Urography

MRI urography provides exquisite detail of the kidneys, ureters, and bladder with no radiation exposure. However, there are many differences between MRI urography and dynamic radionuclide scintigraphy. Dynamic renal scintigraphy,

including diuretic renography when indicated, takes approximately 50 min to complete, while MRI urography requires approximately 1.5 h and typically requires sedation to acquire satisfactory images. For MRI urography, Ga-DTPA (0.2 mL/kg) is infused intravenously for approximately 30 s, while less than 1 nmol of ^{99m}Tc-MAG3 is given as a rapid bolus of <0.2 mL. Furosemide is given approximately 30 min before the administration of the MRI contrast agent in all patients, while in dynamic scintigraphy, furosemide is given only as needed.

Imaging: Diuretic Renography

Prior to administration of the diuretic, it is important to ensure that radiotracer has filled the renal pelvis. In a poorly functioning and severely hydronephrotic kidney, tracer may not be detected by 20 min within a very dilated renal pelvis. If this is the case, it is prudent to wait a few minutes to allow the renal pelvis to fill in with tracer and then proceed with the administration of furosemide. This may or may not resolve the diagnosis. Forced hydration has been suggested as a means to improve the diagnosis of obstruction versus non-obstruction by diuretic renography [37–39]. A compliant and dilated renal pelvis of a poorly functioning kidney leads to one of the pitfalls of diuretic renography: it may not be possible to differentiate a dilated compliant pelvis from obstruction.

The computer is set to record at a rate of 15 seconds per frame for 30 minutes in a 128 x 128 matrix format. The dose of furosemide (1.0 mg/kg, maximum dose 40 mg) is prepared and readied for intravenous injection. Image acquisition is begun 1 min prior to the administration of the diuretic; the initial images can serve as a baseline. The furosemide then is slowly injected over 2 min through the intravenous line. The diuretic effect is very rapid and it is usually seen on the renal time-activity curve by 1–2 min after administration of the furosemide.

In some patients, the forced diuresis causes or reproduces flank pain, especially in those with hydronephrosis who complain of intermittent pain. In some cases, rapid overdistention of the renal pelvis may disrupt the status of a system in which urine flow and drainage are otherwise balanced. In most cases, even with collecting system dilation, rapidly increased diuresis causes no pain or discomfort.

Processing and Display

An integrated display of the entire renogram is useful for interpreting the study as well as helpful in providing the referring physicians with a simple, intuitive, and consistent way to communicate the results (Fig. 12.2).

The Renogram: Interpretation

Interpretation of Renal Radionuclide Angiography

The radionuclide angiogram can be viewed as a series of sequential images or in a cinematic mode. The series of images depict tracer activity as it initially circulates within the aorta and the arterial-arterio territories of the kidneys. However, once tracer reaches the kidneys, dilution will make it difficult or impossible to differentiate the arterial, capillary, and venous phases. Rapid changes in renal blood flow secondary to sudden increases in pressure in the renal pelvis can be detected by radionuclide angiography. This suggests that there can be reversible changes in renal blood flow responding to acute changes in pelvic pressure (Fig. 12.3) [40, 41].

Interpretation of the Renogram

When interpreting a dynamic renal study such as the renogram, it is important to evaluate all the available information including both the images and the time-activity curves derived from appropriate regions of interest (ROI). Cinematic display of the images can be helpful for interpretation by the nuclear medicine physician and the referring physicians. Appropriate

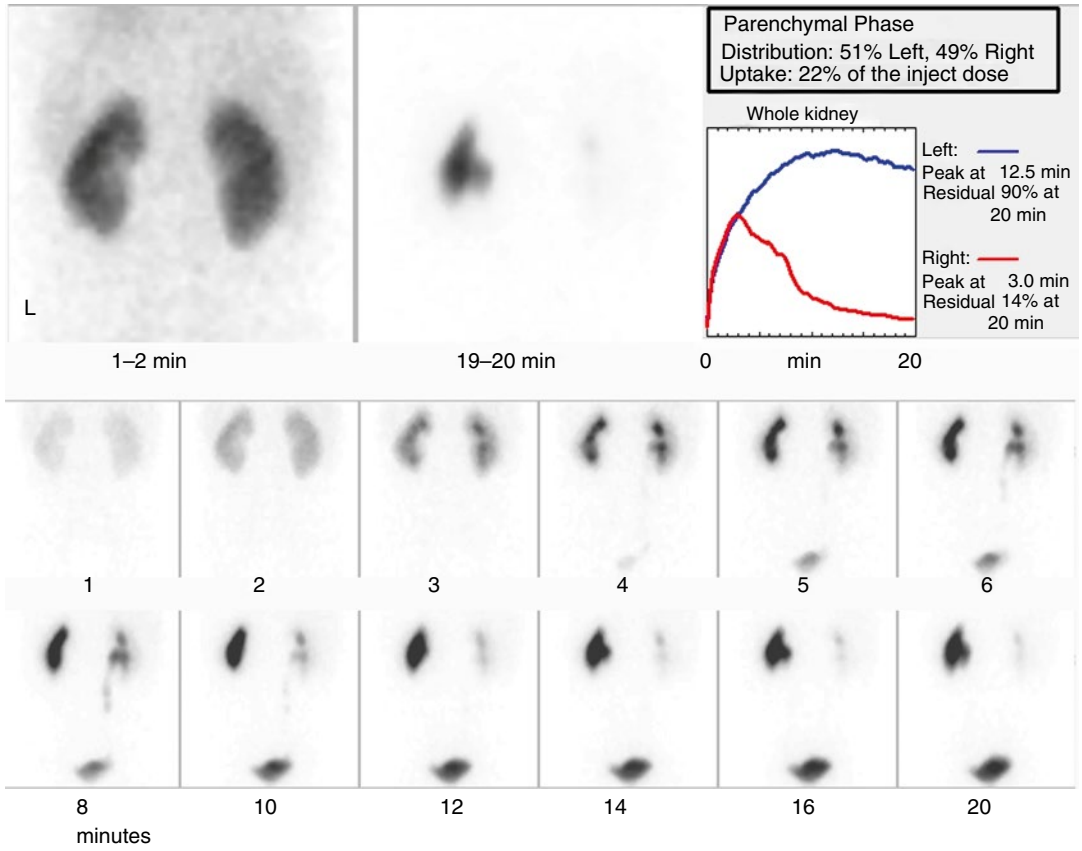

Fig. 12.2 Simplified display developed at Boston Children's Hospital. All information from the parenchymal phase of the renogram can be reviewed on a single screen. Summed dynamic images acquired over twenty minutes are displayed in the *bottom panel*. The are no segmental perfusion defects and cortical transit is identified by three minutes in both kidneys. The right kidney has normal uptake, cortical clearance, and collecting system drainage. The left kidney has normal uptake and cortical clearance, but markedly delayed collecting system drainage. Differential function determined during the second minute of imaging (*top left panel*) is 51 % left kidney and 49 % right kidney. The time activity curve and summary data are displayed in the *upper right panel*

interpretation of the renogram should include a systematic evaluation of three phases of the study. These include:

1. Parenchymal or cortical phase
2. Cortical transit time
3. Urine drainage phase

Parenchymal Phase

The parenchymal or cortical phase occurs after the initial vascular distribution of the tracer and before the first appearance of tracer in the renal collecting system. During this period, tracer concentrates in the renal cortical parenchyma while the blood level of tracer is decreasing. The parenchymal phase provides information about (a) total renal function, (b) split or differential renal function, (c) size and position of the functional renal parenchyma, and (d) renal morphology of functioning renal parenchyma. The parenchymal phase image usually is acquired during the second minute (60–120 s) following the intravenous administration of the tracer (Fig. 12.4).

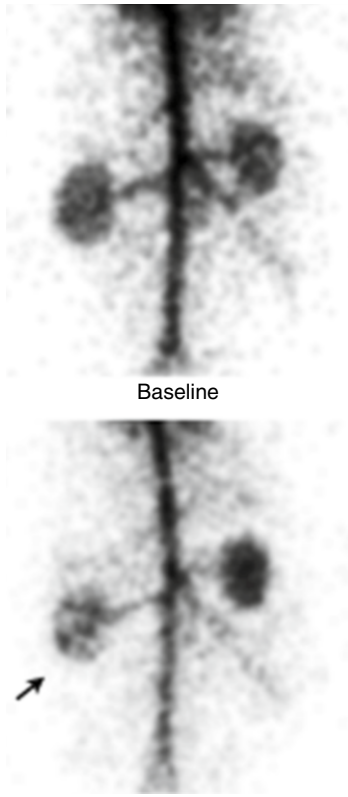

Fig. 12.3 Effect of acute increases in hydrostatic pelvic pressure on renal blood flow. Iridium-191m radionuclide angiograms, 2-s frames. *Top*: Baseline study reveals symmetric renal blood flow. *Bottom*: Decreased left renal blood flow (*arrow*) during acute increase of hydrostatic pressure in the left renal pelvis

Total Renal Function

Evaluating the ratio of the total renal uptake of ^{99m}Tc-MAG3 and the body background activity, one can obtain a qualitative estimate of *total renal function*.

A quantitative estimate of the total renal uptake of the injected dose complements this visual assessment. This can be useful in the serial evaluation of individual patients as the analog images may vary in intensity.

Total renal uptake can be estimated using the following procedure. The syringe containing the tracer to be injected is placed at 15 cm from the face of the collimator using a specially made plastic holder and the activity is recorded as the initial dose. All materials used for the injection of the tracer (e.g., syringe, butterfly needle) are saved for later counting. The dynamic study is recorded as described above. At the end of the dynamic study, the saved materials are placed in front of the collimator using the same holder, and another image (residual dose) is recorded. The total renal counts are determined in regions of interest (ROIs) drawn around the kidneys on the parenchymal phase (60–120 s). All measurements are corrected for background and radioactive decay. Results are expressed as percentage of the administered dose (initial minus residual) in the kidney(s) during the parenchymal phase.

As this approach does not correct for tissue attenuation and depth, only an estimate of the total renal uptake is obtained, not an absolute value. Meticulous attention to detail and study-to-study consistency are essential to avoiding errors that may lead to inadequate assessment of renal function. We evaluated the normal values of estimated percentages of the injected dose in the kidneys using our method in children. The estimated percentage of the total renal uptake of the injected dose in children younger than 5 years of age (range 1–60 months) with normal total renal function ranged from 8 to 23 % with an average of 15.4 % (median 15.0 %, range 8–23 %). These children's weights averaged 10.1 kg (median 8.0 kg, range 5–23 kg), serum creatinine levels averaged 0.3 mg/dL (median 0.2 mg/dL, range 0.2–0.4 mg/dL), and serum BUN levels averaged 11.7 mg/dL (median 10 mg/dL, range 5–18 mg/dL).

Split or Differential Renal Function

The parenchymal phase provides information about *differential renal function (split renal function)*. The differential renal function can be calculated in the parenchymal phase from the ratio of counts from the corresponding ROI from each kidney. This ratio is consistent with a differential

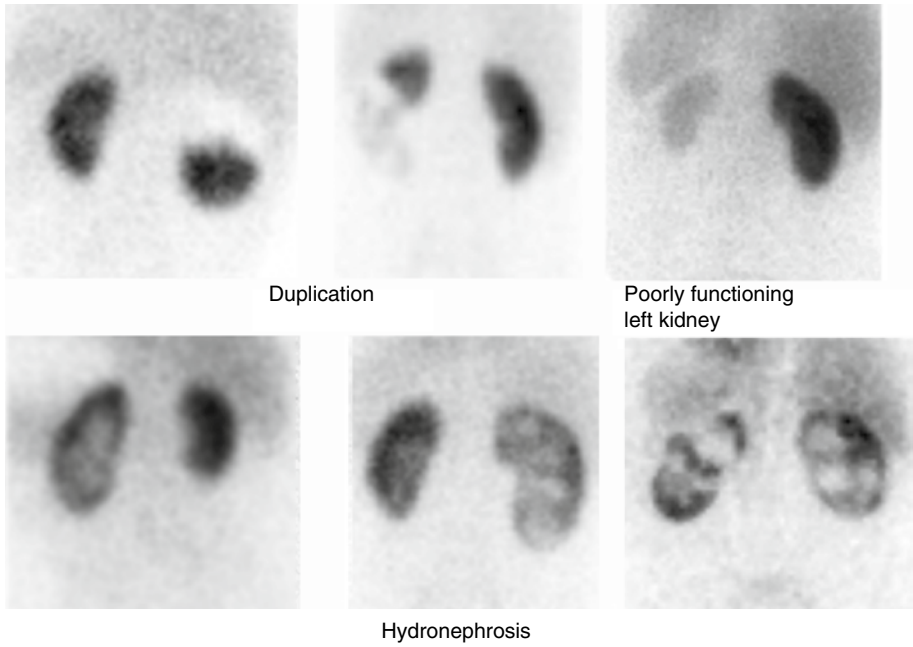

Fig. 12.4 Examples of ^{99m}Tc-MAG3 parenchymal phase images. *Top left* and *middle*: Two examples of renal duplication. *Top right*: Poorly functioning left kidney. *Bottom left*: Left hydronephrosis. *Bottom middle*: Right hydronephrosis. *Bottom right*: Bilateral hydronephrosis

renal function calculation that can be obtained from renal ^{99m}Tc-DMSA scintigraphy when the function in each kidney is greater than 10–15 % of the total renal uptake. If the renal function from an individual kidney estimated by ^{99m}Tc-MAG3 is less than 10–15 %, then this method likely will underestimate of the kidney's contribution to the total renal function. This likely is due to slow accumulation of tracer over many minutes in a kidney with markedly impaired function, as well as difficulty discriminating low levels of renal uptake from background. In these cases, ^{99m}Tc-DMSA scintigraphy will provide a more reliable determination of differential renal function.

Placement of ROIs over the kidneys without including extraparenchymal sources of activity may be difficult, especially in cases of poor renal function and in hydronephrosis. Careful attention to detail and consistency during selection of background ROIs is essential as different sizes and positions of background regions can produce different results. This can be most problematic when the renal function is low or hydronephrosis is present. Thus, it is crucial to verify any semiquantitative results with visual assessment.

Kidney Size and Position

The *relative renal size* can be estimated by simple visual observation of the parenchymal image. The maximum renal dimensions in the longitudinal and transverse planes can be measured with a calibrated system or by imaging a radioactive ruler placed to the side of the patient. In addition, the *functional size of the kidneys* can be estimated by comparing the kidneys with the body outline and relative proportions of visible organs on early images. However, this assessment is not as accurate as can be obtained with renal cortical scintigraphy. The parenchymal phase also shows the *position of the kidneys*. If a pelvic kidney is

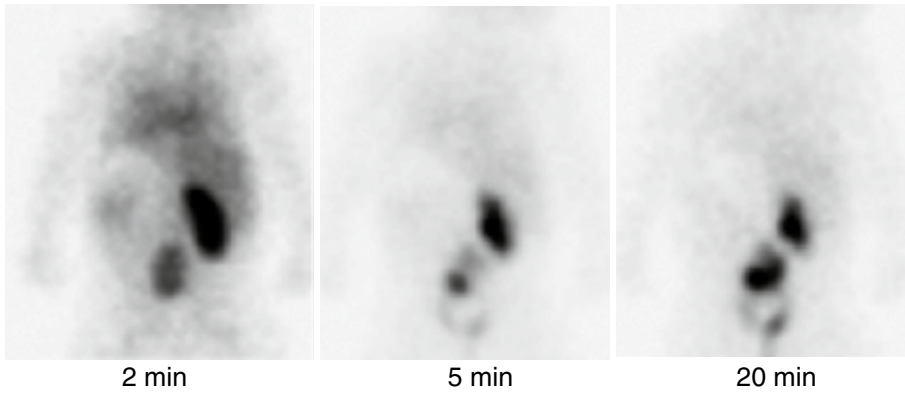

Fig. 12.5 Ectopic left kidney. ^{99m}Tc-MAG3 renogram demonstrates tracer uptake renal parenchyma of a normally positioned right kidney and ectopic pelvic right kidney on the 2-min image. By 5 min, tracer appears in the renal pelvis of both kidneys. The right kidney demonstrates persistent tracer accumulation in the collecting system, concerning for mild ureteropelvic junction obstruction

suspected, it is important to include the pelvic area within the field of view of the camera (Fig. 12.5).

Morphology of Functioning

Renal Parenchyma

The parenchymal phase provides information about *overall morphology of the kidneys* and intrarenal distribution of radiotracer. In kidneys with pelvicaliectasis or hydronephrosis the funtional cortex appears as a rim of uptake around the dilated renal pelvis. Larger cortical defects and some renal scars also can be identified, such as a malfunctioning upper pole in a duplex kidney, trauma, tumor, or cyst. The parenchymal phase does not allow detection of small cortical defects, however.

Cortical Transit Time

A very useful parameter that can be measured from the dynamic renal study is the *cortical transit time*. The cortical transit time can be defined as the time between the intravenous administration of the tracer and the first appearance of tracer within the renal collecting system. With normal renal function radiotracer should appear within the renal collecting system 2–5 min after intravenous injection. With impaired renal function, the cortical transit time will be prolonged. In the presence of pelvicalyceal dilation, a normal cortical transit time can be reassuring that there has been little loss of renal cortical function. As the tracer is excreted from the renal cortex into the renal pelvis, parenchymal renal activity should decrease gradually. Even if the cortical transit time appears to be within the normal range, it is important to confirm that it is associated with a decrease of parenchymal activity. Cortical transit time may be prolonged in several conditions that affect renal function, including renal immaturity, ureteral obstruction, hydronephrosis, renal insufficiency, acute tubular necrosis, renal artery stenosis, renal vein thrombosis, acute and chronic pyelonephritis, transplant rejection, nephrotoxicity, and trauma.

Urine Drainage Phase. As the renogram progresses to the *drainage phase*, tracer gradually is eliminated through the pelvicaliceal system and the ureters into the bladder. By the end of the 20 min renogram, nearly all of the tracer should have cleared from the renal parenchyma and most should be drained from the renal collecting system. Time-activity curves generated from regions of interest over an entire kidney usually reveal peak activity at 4–6 min with subsequent decrease by 20 min. With normal renal function and drainage, the twenty-minute residual should be less than 50 % and usually is less than 35 %. Time-activity curves must not be interpreted alone, but along with careful evaluation of the images of the parenchymal phase, cortical transit,

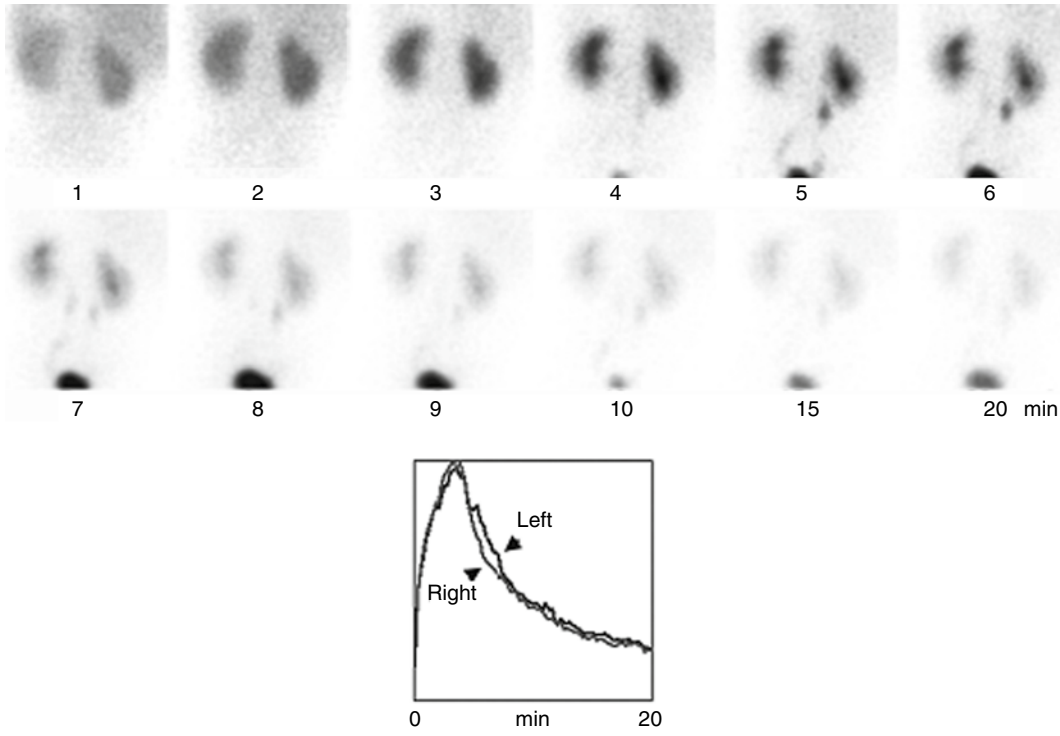

Fig. 12.6 Normal ^{99m}Tc-MAG3 renogram in a 4-week-old girl with a question of renal obstruction. Dynamic images acquired for twenty minutes after tracer administration demonstrate symmetric tracer accumulation in both kidneys. By four minutes, there has been cortical transit of tracer and tracer accumulation is seen in both ureters and the bladder. The is rapid drainage of the collecting system. The time activity curve (*bottom panel*) confirms these findings. Maximal activity is at 4 minutes in both kidney, and the curves demonstrate a normal concave appearance during the drainage phase. By twenty minutes, residual tracer in each kidney is 20–25 %

and the drainage phase. A normal cortical transit time with nearly complete cortical clearance of the tracer from the cortex at 20 min accompanied with a renal time-activity curve that reveals a delayed peak and high residual value indicates delayed urine drainage without parenchymal dysfunction. The most accurate interpretation requires examination of both serial images and time-activity curves.

A *normal dynamic renal study* reveals relatively rapid and intense concentration of the tracer in the renal parenchyma at 1–2 min after administration (Fig. 12.6). Passage of the tracer into the renal calyces and the renal pelvis occurs at 3–5 min. In the absence of ureteral dilation or obstruction, visualization of tracer in the ureters is variable. The ureter may be visualized in some normal patients and those with slow ureteral transit time. Ureteral dilatation or very slow transit time, with or without obstruction, usually shows as ureteral visualization in the renogram. By 20 min after injection, the radiotracer usually has cleared almost completely from the renal parenchyma. Small residual amounts of tracer persisting in the pelvicaliceal system at 20 min may be normal and are usually of no clinical significance. Minimal residual tracer tends to clear spontaneously, with a change in the patient's position or after voiding. Tracer appears within the bladder 3–6 min after injection, and its level increases with time as more of it is excreted by the kidneys. In a patient with normal renal function, soft-tissue background, which reflects blood clearance of the tracer and therefore total renal function, rapidly decreases with time.

If there is no retention of tracer within the pelvicaliceal system or the ureter(s), the study is terminated at 20 min. If, at the end of the initial 20 min, tracer is retained within the pelvicaliceal system, the patient should be encouraged to get up, void in the bathroom, and walk around for a few minutes if possible (a small child should be picked up for a few minutes) to promote postural drainage. An additional image is then obtained to determine if drainage has occurred. Kidneys that drain with a change in patient position should not be considered obstructed [42]. If urinary obstruction is suspected, a diuretic renogram may be indicated (see below).

Interpretation of the Diuretic Renogram

Intravenous administration of furosemide is followed by a rapid diuretic response that displaces tracer from dilated unobstructed systems. If there is significantly obstruction of the collecting system, then tracer in the renal area decreases slowly, fails to decrease, or even increases in response to the induced diuresis.

In diuretic renography, drainage is directly proportional to urine flow and inversely proportional to the volume of the renal pelvis and ureter. Urine flow depends on the level of renal function and amount of renal parenchyma present, as well as the ability of the parenchyma to respond to the diuretic. There are a set of factors that, when present, limit the ability of diuretic renography to determine if there is obstruction or not. These pitfalls include poor renal function; parenchymal loss; large, flaccid, and compliant renal pelvis and/or ureter; infiltration of the diuretic; bladder overdistention; prune-belly syndrome; and complex surgeries [43–45].

Interpretation of the diuretic study must include the evaluation of both the initial 20-min dynamic renal study and the diuretic phase.

In the absence of obstruction, rapid and almost complete washout of radiotracer from the pelvicaliceal system occurs. If a kidney drains satisfactorily during the initial dynamic renal study, half-time ($t_{1/2}$) is not calculated. As there is not much tracer remaining, a calculated $t_{1/2}$ will be prolonged and potentially misleading. In obstructed systems, drainage of tracer following administration of the diuretic is slow and there is tracer retention at the end of the study. Interpretation of intermediate diuretic renographic patterns can be more difficult.

A comparison is made of images obtained prior to the administration of the diuretic and at the end of the 30-min diuretic study. The diuretic washout $t_{1/2}$ is determined using a mono-exponential interpolation between a point on the initial descent of the time-activity curve and another point on the downslope while the curve is decaying monotonically. A rapid initial $t_{1/2}$ can be followed by significant retention of tracer in the renal pelvis. Therefore, it is important to report both the initial washout $t_{1/2}$ and the residual activity in the renal pelvis at 30 min.

Estimation of the diuretic half-time is a useful adjunct to the assessment of urinary obstruction. Washout half-time has been overemphasized as the only factor in the assessment of possible kidney obstruction. This approach can lead to oversimplification of a rather complex condition as diuretic half-time is only one of several factors considered when assessing urinary obstruction.

At least three different methods have been used to calculate the diuretic washout half-time. Therefore, diuretic half-time values vary from method to method and from observer to observer (Fig. 12.7). Despite these variations in technique, the overall sensitivity of diuretic renography for the detection of obstruction in children remains high [46].

Advanced Image Processing

Advanced planar processing software provides opportunities to decrease administered radiopharmaceutical dose while maintaining or improving the quality of planar images. Research in our laboratory has shown that the administered dose of ^{99m}Tc-MAG3 can be reduced to 2.2 MBq/kg (0.06 mCi/kg) without compromising image quality when images are viewed at 1 frame per minute. With noise reduction software, the administered dose can be reduced further to 1.5 MBq/kg (0.04 mCi/kg). Denoising software may permit a significant reduction in administered radiopharmaceutical dose and patient radiation

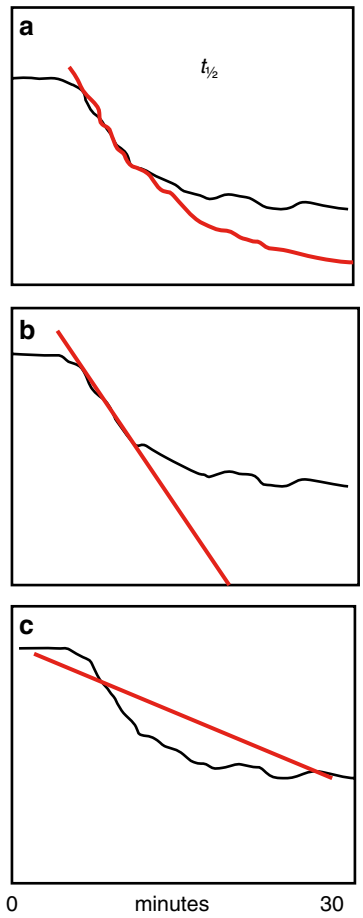

Fig. 12.7 Different ways of calculating diuretic-phase half-time from the diuresis time-activity curve: (**a**) Exponential interpolation of the washout curve in the region of fastest collecting system drainage may provide the most accurate assessment of collecting system obstruction, (**b**) Linear interpolation in the region of fastest collecting system drainage, (**c**) Linear interpolation from time 0 to the end of imaging at 30 minutes may be the least accurate

exposures without loss of diagnostic information. (Fig. 12.13) [17].

Renal Cortical Scintigraphy

Patient Preparation

There is no need for special patient preparation for this method other than informing the patient and caregivers of what to expect in terms of the method and the several hours of time commitment from arrival, tracer injection, and imaging. In our experience, sedation is used rarely, if ever, for this procedure.

Radiopharmaceutical and Administered Doses

^{99m}Tc-DMSA

Technetium-99m-DMSA is the agent of choice for renal cortical imaging by planar scintigraphy, by pinhole magnification, or by single photon emission computed tomography (SPECT). Technetium-99m-DMSA is administered intravenously with a usual dose of 0.05 mCi/kg (1.85 MBq/kg) [minimum 0.3 mCi (11.1 MBq); maximum 3.0 mCi (111 MBq)]. After intravenous injection, this agent is 90 % bound to plasma proteins, and a small amount (0–5 %) is associated with red cells [47]. In normal individuals, the blood disappearance of ^{99m}Tc-DMSA follows a single exponential with a mean half-time of 56 min and with 6–9 % of the administered dose present in the blood at 14 h after injection. The renal uptake of ^{99m}Tc-DMSA is approximately 40–50 % of the injected dose at 4 h and 70 % at 24 h, [47, 48]. Most accumulated tracer is found in the proximal convoluted tubules, with small amounts elsewhere in the kidney (Fig. 12.8) [49]. Although most ^{99m}Tc-DMSA is retained in the renal parenchyma, cumulative urinary excretion has been reported to be 6 % at one hour, 1–12 % at two hours, and 25 % at 14 hours.

The distribution of ^{99m}Tc-DMSA uptake between kidneys reflects regional renal blood flow and functional renal parenchymal mass [50, 51, 52]. There is an autoregulation phenomenon that maintains total renal function at normal levels even in an increase in the number of nephrons and apparent renal mass. For example, in experimental rats receiving a renal transplant, the animal ends up with three kidneys (two native and one transplant), and the total renal uptake of DMSA remains the same as before transplantation. The tracer is evenly distributed among the three renal units. There appears that there is a feedback signal to enable the aggregate renal

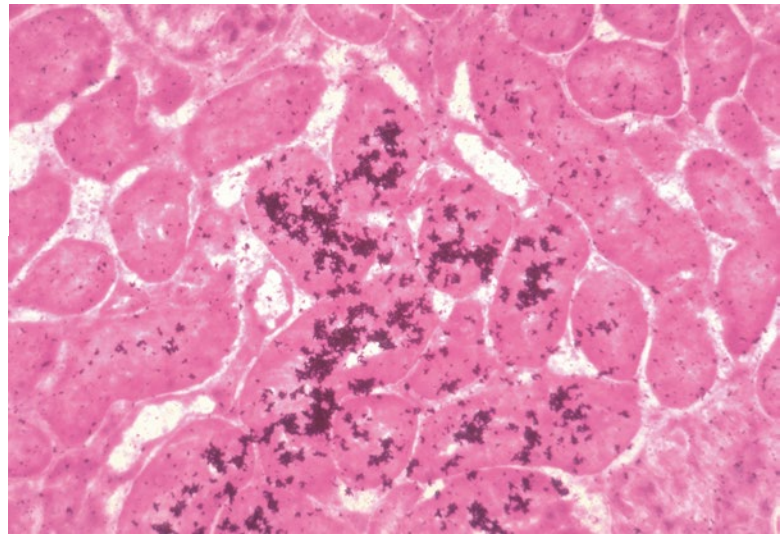

Fig. 12.8 ^{99m}Tc-DMSA. Frozen section autoradiography from a rat kidney 1 h after intravenous injection of ^{99m}Tc-DMSA. Tracer concentrates principally in the proximal convoluted tubules. Minimal or no tracer activity is seen elsewhere

Fig. 12.9 Three-kidney rat 16 h after injection of DMSA. The transplanted third kidney (T) lies below the other two [53]

glomerular and tubular clearance to remain a constant linear function of body weight even in the presence of an additional kidney (Fig. 12.9) [53].

In patients, excellent images of renal cortex can be obtained approximately 3–4 h after administration of ^{99m}Tc-DMSA. In patients with obstruction, tracer retained within the pelvicaliceal system can interfere with mapping of functioning renal parenchyma and may lead to the wrong estimate of differential renal function. It is important to evaluate carefully the images acquired at 4 h to confirm that there is no tracer in the pelvicaliceal system. If tracer is retained, later imaging (up to 24 h after injection) may allow tracer in the urine to be eliminated and permit a better assessment of renal cortices and differential renal function (Fig. 12.10).

Renal Scintigraphy: Imaging

Three to four hours after administration of ^{99m}Tc-DMSA, the kidneys may be imaged using planar scintigraphy, pinhole magnification, or SPECT.

Planar Renal Scintigraphy

Planar renal scintigraphy can provide information about: (1) number, position, size, and overall morphology of the functioning kidneys; (2) differential renal function; and (3) regional parenchymal function. For conventional planar renal scintigraphy the patient is examined in the supine position, and a posterior image containing 300,000–500,000 counts is recorded using a high-resolution or, preferably, ultrahigh-resolution

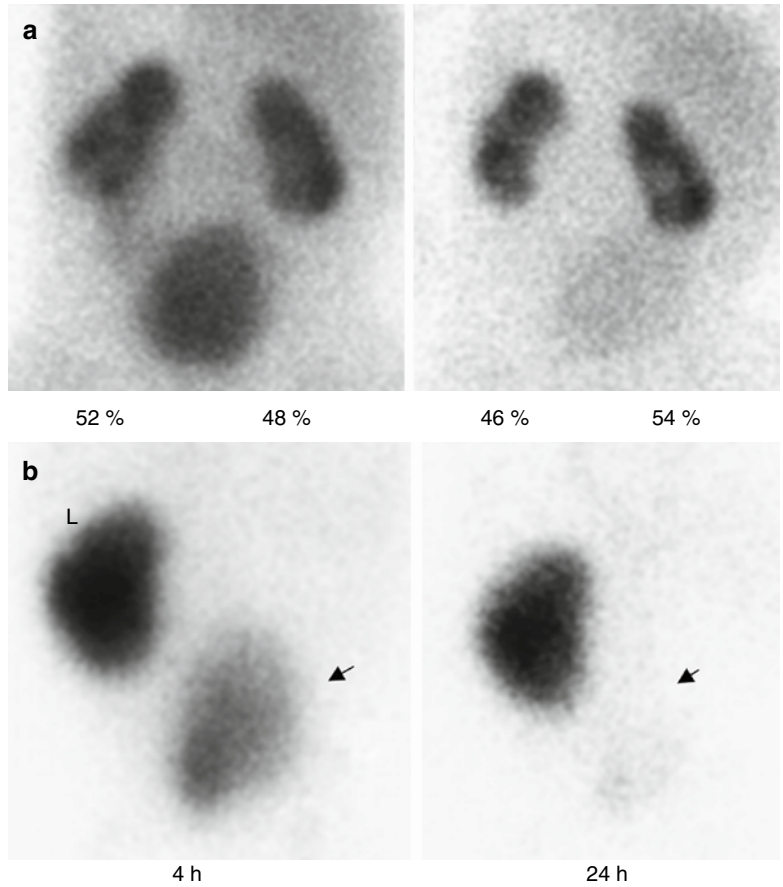

Fig. 12.10 (**a**) 4-day-old infant with bilateral hydronephrosis, hydroureters, and severe bilateral reflux. *Left*: The 4-h image estimates a 52 %–48 % differential ^{99m}Tc-DMSA uptake. However, high levels of tracer in the pelvis and ureters interfere with assessment. *Right*: An image at 24 h is clear of excreted urinary activity and best represents the differential renal function as 46 %/54 %. (**b**): ^{99m}Tc-DMSA cortical scintigraphy in a 3-month-old boy with nonvisualization of the right kidney by ultrasonography. This study was performed to look for any evidence of right renal function. *Left*: Scintigraphy at 4 h revealed normal tracer accumulation in the left kidney (*L*). Tracer accumulation in the right side could correspond to an ectopic right kidney or tracer in the bladder (*arrow*). *Right*: Image at 24 h shows clearance of tracer from the pelvis, which clearly demonstrates that tracer had accumulated in the bladder (*arrow*) with, no evidence of an ectopic pelvic right kidney

collimator on a 256 × 256 matrix format. Left and right posterior oblique projections may be useful for identifying cortical defects. A calibrated system enables measurement of the size of the functional renal parenchyma. Semi-quantitative assessment is performed with regions of interest of each kidney and background areas. The differential split renal uptake corrected for body background is then calculated. The normal differential renal uptake is nominally 50 %/50 % (+/–5 %), so it can range from 45 %/55 % to 55 %/45 %. In renal duplication, separate regions of interest of the upper and lower poles can be used to estimate the distribution of functioning renal parenchyma with in the duplicated kidney. A more detailed assessment of regional parenchymal function (e.g., scar, inflammation, infarct, duplex) is best done with SPECT or with pinhole magnification.

Magnification Renal Scintigraphy

Pinhole magnification is very effective for detailed imaging of the kidneys in both infants (in whom magnification is essential) as well as older children and adolescents. A pinhole

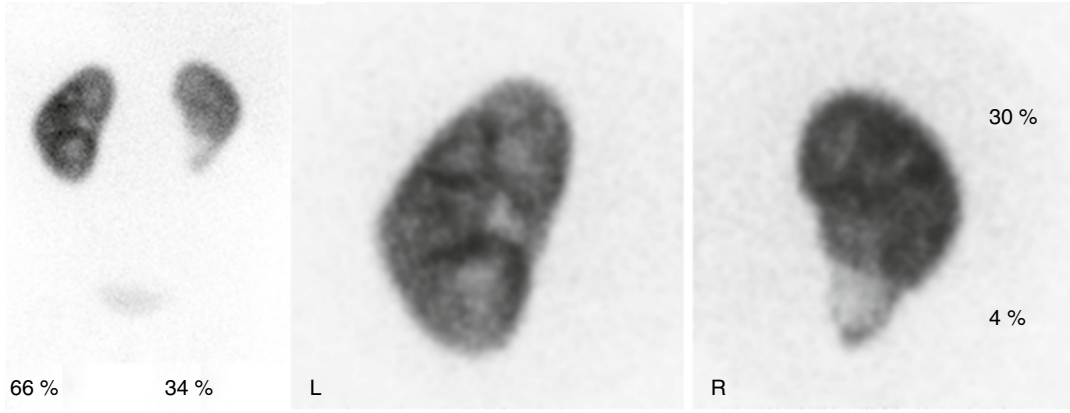

Fig. 12.11 ^{99m}Tc-DMSA pinhole scintigraphy in a 2-year-old girl with repeated urinary tract infections, a double right collecting system, and moderate vesicoureteric reflux in the right lower pole. Posterior images reveal reduced relative function of the right kidney. There is a large cortical in the lower moiety of the right kidney (*left panel*). Pinhole images (*right panel*) reveal greater detail with a clear delineation of the focal reduction of tracer uptake in the right (R) lower moiety. Region of interest analysis showed that the upper moiety contributes 30 % of total renal function, while the lower moiety contributes only 4 % of total renal function

collimator with an internal diameter of 2–3 mm provides images of high spatial resolution (2–3-mm range). Posterior and posterior oblique projections are useful to detect and outline cortical abnormalities. Each pinhole image is obtained for approximately 150,000 counts using a 256×256 matrix (Figs. 12.11 and 12.12). Cortical functional defects in pyelonephritis, infarction, scarring, duplication and fetal lobations can be discerned better with pinhole magnification than with parallel-hole, high resolution collimators.

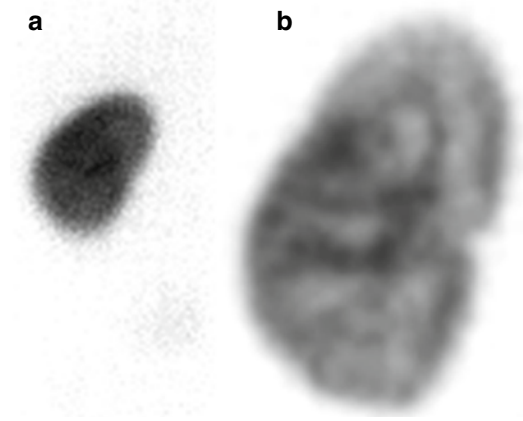

Fig. 12.12 Right multicystic dysplastic kidney. The right kidney is not visualized. Planar (**a**) and magnified pinhole images (**b**) are shown. Note the detailed visualization of renal cortex on the pinhole image

Advanced Image Processing

Advanced planar processing software provides opportunities to decrease administered radiopharmaceutical dose while maintaining or improving the quality of planar images. Denoising software may permit a significant reduction in administered radiopharmaceutical dose and patient radiation exposures without loss of diagnostic information. (Fig. 12.13) [17].

Single Photon Emission Computed Tomography (SPECT)

Technetium-99m-DMSA single photon emission computed tomography (SPECT) is superior to conventional planar or pinhole scintigraphy for mapping regional functioning renal parenchyma. By definition, SPECT permits simultaneous evaluation of images in the transverse, coronal, or sagittal plane, or in any plane. Evaluating rotating volume-rendered images permits a superior overall view of the functional anatomy of the kidneys. Using modern systems, renal SPECT

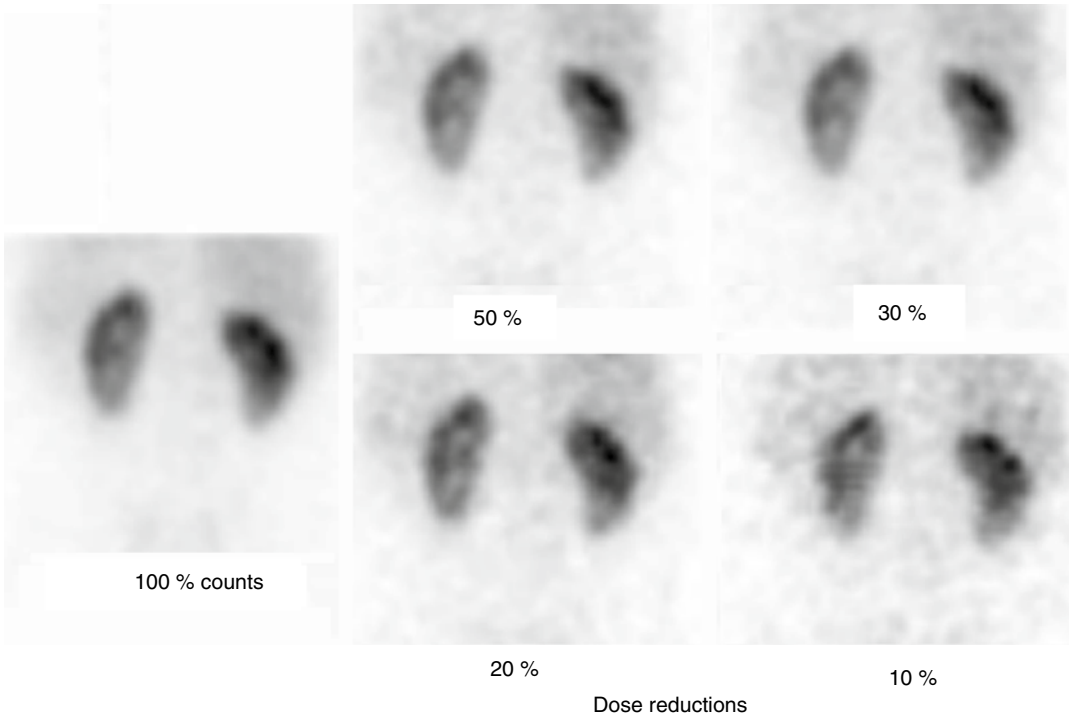

Fig. 12.13 Dose reduction using advanced image processing. Simulated noise was added to simulate fewer counts/activity. Then, spatially variant filtering was used for noise reduction, demonstrating that advanced image processing may permit high image quality with lower radiopharmaceutical doses [183]

acquisition requires 15–20 min (Figs. 12.14, 12.15, and 12.16). SPECT may be less suitable for small patients less than 1 year of age. With currently available SPECT cameras, the detectors cannot easily be positioned close to a small patient and the distance between the cameras and kidneys limits detailed renal imaging.

Iterative Reconstruction

Until recently, most renal SPECT studies have been processed using the technique of filtered back projection. The application of 3-D Ordered Subset Expectation Maximization (OSEM) with resolution recovery (for example, OSEM 3D, Flash 3D, Siemens) can result in a significant improvement in DMSA image quality compared to filtered back projection. The improved image quality can facilitate a reduction of radiopharmaceutical administered doses and, therefore, reduction in radiation exposure. Alternatively, utilization of OSEM may permit a substantial reduction in acquisition time without loss of image quality (Figs. 12.17 and 12.18) [54].

Measurement of Renal Volumes with SPECT

Measurement of individual renal volumes in children can be elegantly performed with an automated method of SPECT analysis. With this method, we measured renal volumes in 310 children without renal disease with a median age of 8.8 years (range 1–21 years of age). This automated approach showed a high level of reproducibility and reliability compared to other methods. Normal ranges of renal volumes in children were determined with this method. These volumes were determined as a function of body weight in males and females (Fig. 12.19) [55].

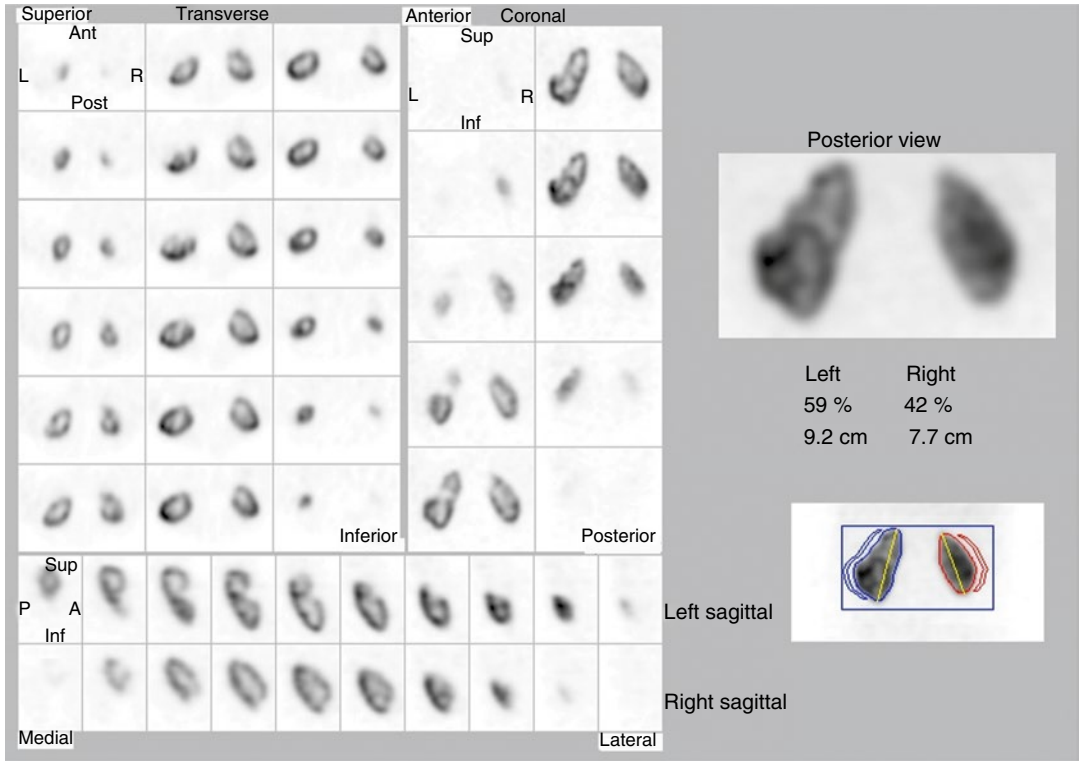

Fig. 12.14 ^{99m}Tc-DMSA SPECT in a 9-year-old female with hypertension and with normal ultrasonography with Doppler. Summed projection images are used to determine that differential renal function is left 59 % and right 42 %. The left kidney has an irregular contour and the right kidney is smaller than the left. In the *left panel*, slices in the transverse, coronal, and sagittal projections more clearly delineate cortical defects the in the lateral mid and superior aspect of the left kidney

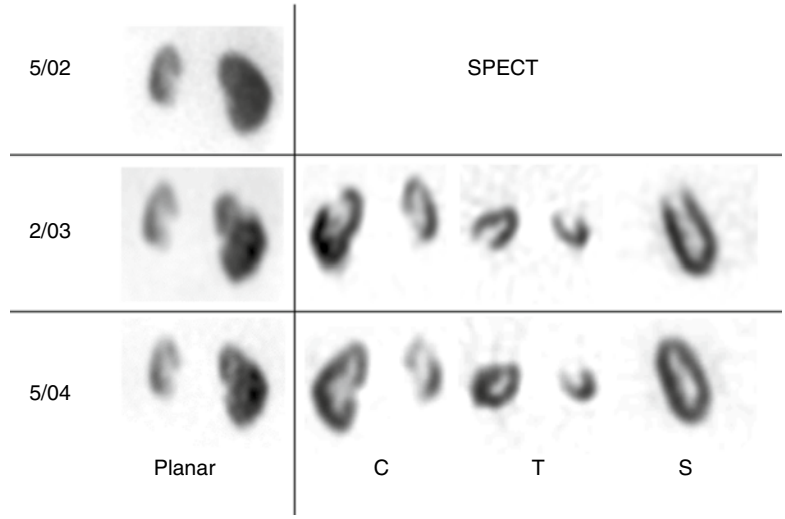

Fig. 12.15 Pyelonephritis and recovery. Planar and SPECT ^{99m}Tc-DMSA images of a 7-year-old girl with bilateral vesicoureteral reflux. Planar images reveal the left kidney has lower renal function and that on 2/03 a cortical defect was present in the right upper pole. SPECT reveals the defect more clearly. Following a course of intravenous antibiotics, the defect has largely resolved. This recovery is more clearly seen on SPECT. *C* coronal, *T* transverse, *S* sagittal

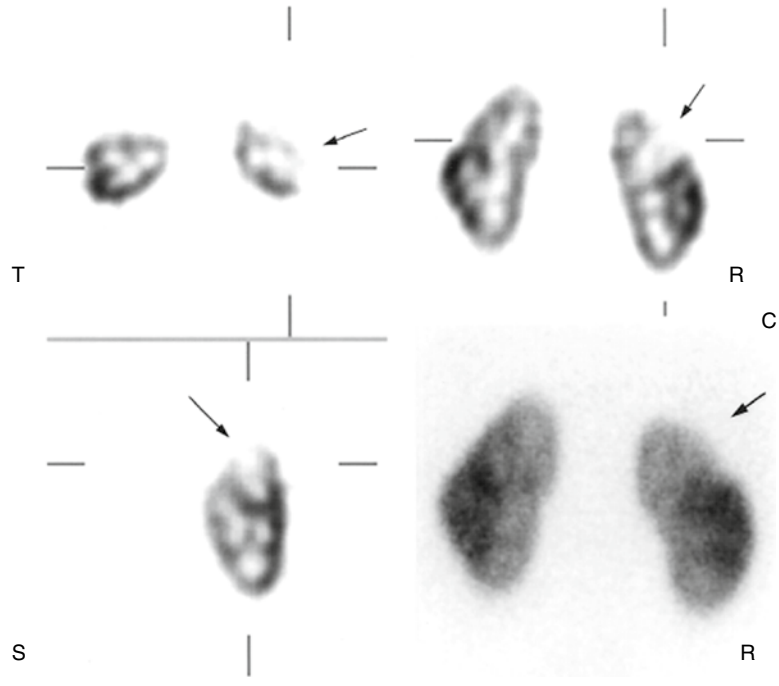

Fig. 12.16 Single photon emission computed tomography (SPECT) and conventional planar scintigraphy in pyelonephritis. This 16-year-old girl with a history of repeated urinary tract infections and vesicoureteric reflux presented with acute onset of right flank pain and fever. Selected transverse (*T*), coronal (*C*), and sagittal (*S*) slices reveal a focal cortical defect in the right upper pole (*arrows*). Conventional planar scintigraphy does not show the defect (*arrow*) as clearly as SPECT

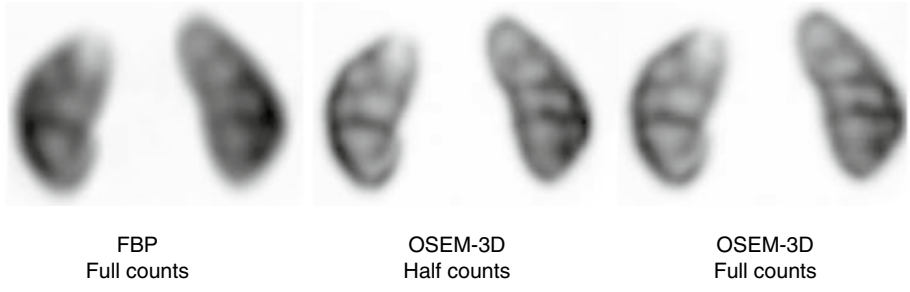

Fig. 12.17 OSEM 3D (Ordered Subset Expectation Maximization) with resolution recovery [54]. *Left*: DMSA SPECT reconstructed with Filtered Back Projection (FBP). *Middle*: Same image with 50 % counts reconstructed with OSEM 3D. *Right*: Same image with 3D OSEM containing full counts

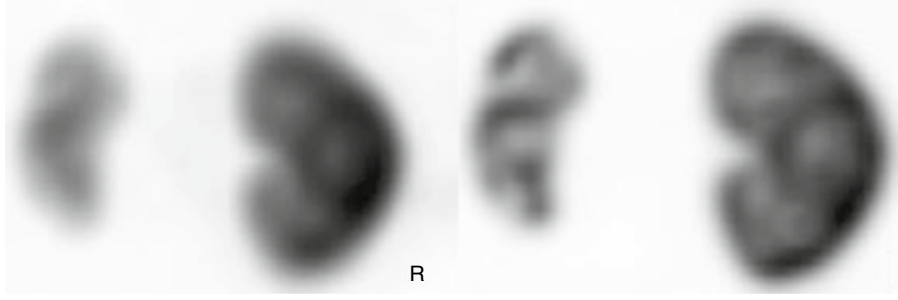

Fig. 12.18 Effect of OSEM 3D and resolution recovery on DMSA SPECT [54]. *Left*: DMSA SPECT reconstructed with Filter Back Projection. *Right*: DMSA SPECT reconstructed with OSEM 3D with resolution recovery

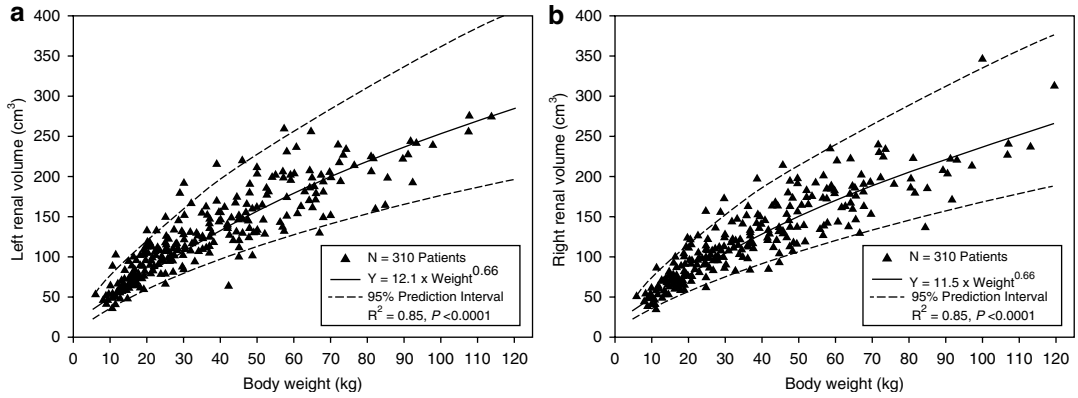

Fig. 12.19 Nonlinear relationship (*solid lines*) between renal volume and body weight for left (**a**) and right (**b**) kidneys with 95 % confidence intervals representing the normal ranges (*dashed lines*). The power models fit the empirical data closely. Male and female patients are pooled together because no gender differences were detected for left or right renal volumes [55]

Clinical Applications

Renal Immaturity/Neonatal Period

When evaluating newborn infants, nuclear medicine clinicians should recognize normal renal immaturity and its effect on the renal handling of radiotracers [56]. The glomerular filtration rate (GFR) per unit of surface area in the newborn is approximately 30 % of the adult rate. During the first few days of life, there is a dramatic rise in the renal function, followed by a more gradual increase with adult levels (normalized to BSA) reached at 6 months to 1 year of age. Studies of very low birth weight (VLBW) premature infants have revealed dramatically lower renal function with a much slower rise to normal levels [57].

Most newborns are able to urinate within 24 h from birth. In problem cases, radionuclide imaging is useful to assess renal function, even in the absence of diuresis. The combination of ultrasonography and scintigraphy has proved useful for evaluating renal function in this group of patients.

Depending on renal maturation, renal uptake of dynamic tracers may be lower in newborns than in older children and adults. In addition, intrarenal transit time and excretion of these tracers may be slow at this age. During the first or second week of life, a dynamic renogram may demonstrate faint, delayed renal uptake of the tracer with or without bladder activity at the expected times. If tracer is seen in the bladder within 2–5 min, the amount present may be lower than in older children. Background may be high throughout the study, reflecting low plasma clearance of the tracer. As the child matures and renal function increases, renal uptake, intrarenal transit time, and excretion of tracers reach normal values. Some normal newborns, however, show apparently normal handling of dynamic renal tracers (Fig. 12.7).

Renal function immaturity also may be reflected on ^{99m}Tc-DMSA studies. In normal newborns, there may be relatively low kidney/background ratio. Intravenous urography is not the initial method of choice in this age group because of the poor concentration of contrast agents by the kidneys and the relatively high doses of contrast agents that must be used [58–60].

Hydronephrosis/Obstruction

Hydronephrosis is one of the most common indications for radionuclide evaluation of the kidneys in pediatric patients. Findings on renal scintigraphy vary depending on hydration, age, type, and severity of the disease, site of obstruction, unilateral or bilateral pathology, presence

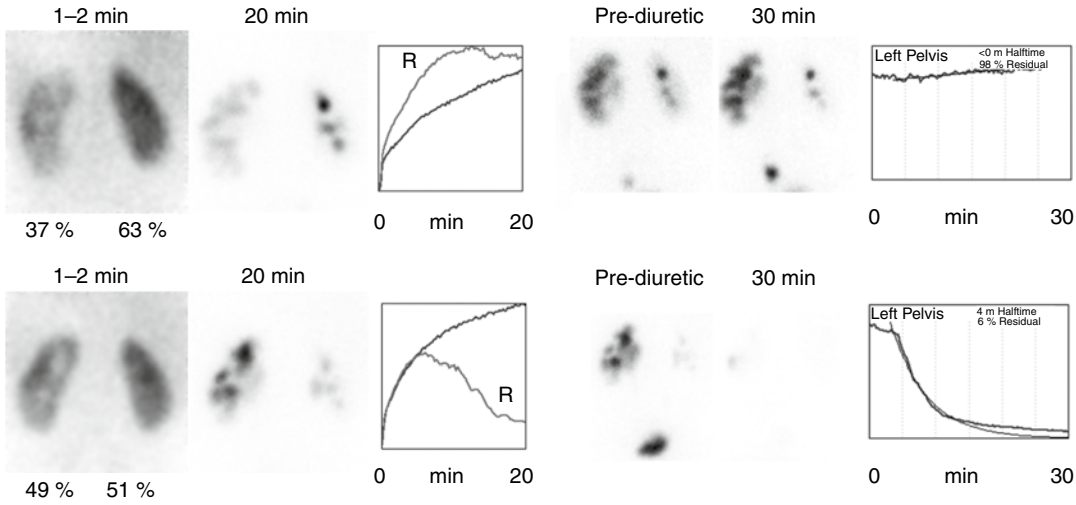

Fig. 12.20 Left hydronephrosis with ureteropelvic junction obstruction in a 2-month-old boy. *Top row*: Preoperative study reveals differential function 37 % left and 63 % right. Both kidneys have mild cortical retention, consistent with immaturity, and markedly delayed spontaneous collecting system drainage. During diuresis, there is prolonged retention of tracer in the left renal pelvis with a clearly obstructive pattern. *Bottom row*: Following left pyeloplasty, differential renal function is 49 % left and 51 % right. With maturation, the right kidney demonstrates a nearly normal time-activity curve. The left kidney still has markedly delayed spontaneous drainage, but during diuresis, there no longer are findings of obstruction (*left*, 49 %; *right*, 51 %)

or absence of reflux, and recent surgery. In cases of hydronephrosis caused by obstruction at the ureteropelvic junction or ureterovesical junction, dynamic renal scintigraphy demonstrates abnormalities in structure and function on the involved side. With posterior urethral valves, there is bilateral renal involvement, and patients who present during early infancy may have severe obstruction with impaired renal function. In young children, the evaluation of function in the presence of obstruction does not give a reliable indication of the potential for recovery. It does indicate, however, the minimal function that may be expected.

In the young, even poor renal function caused by chronic obstruction is potentially reversible [61]. In these patients, ultrasonography should be obtained to search for surgically correctable lesions. Serial renal scintigraphy can be used to assess recovery as renal function may improve once the obstruction has been relieved. In newborn hydronephrosis without obvious obstruction, the hydronephrosis may resolve spontaneously, suggesting that some hydronephrosis in neonates and infants is a manifestation of physiologic change during development [62–66]. Thus, in a young child with hydronephrosis, one should not arrive at the diagnosis of obstruction or prognosis based on a single examination. A single study provides only a "snapshot" of a changing situation. Serial studies over time provide a better indication of the natural progression of the hydronephrosis and help determine the presence of an obstruction (Figs. 12.20, 12.21, 12.22, 12.23, and 12.24).

With dynamic renography a hydronephrotic kidney initially will appear as a rim of tracer accumulating in the renal parenchyma surrounding a dilated collecting system. As dynamic imaging continues, the pelvicaliceal system slowly will fill with tracer. The rate of appearance and the amount of the tracer in the pelvicaliceal system will depend on the cortical function of the hydronephrotic kidney and the degree of collecting system obstruction. Depending on the severity and duration of the obstruction, tracer may begin to accumulate in the renal pelvis within 3–6 min despite severe dilatation; with prolonged severe obstruction, however, tracer accumulation in the dilated renal pelvis is much slower.

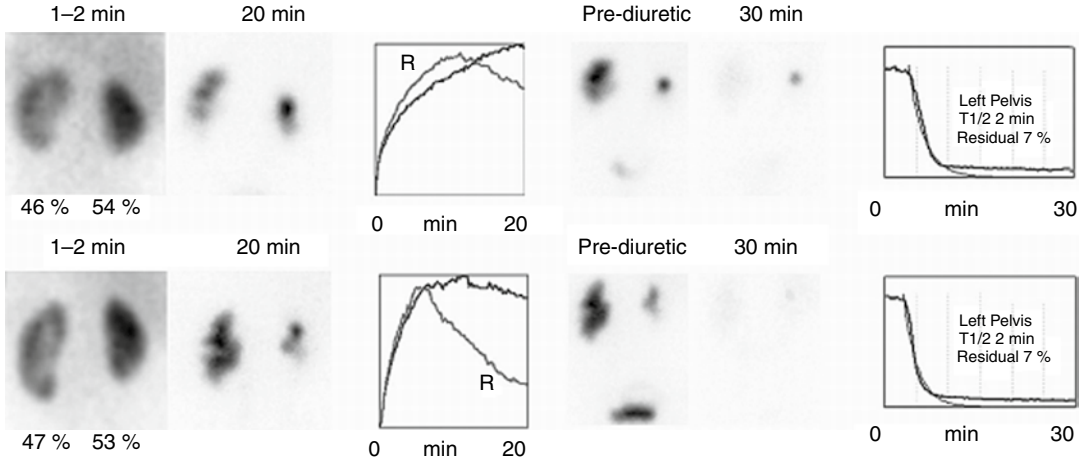

Fig. 12.21 Prenatal diagnosis of left hydronephrosis in a 2-month-old with mild ureteropelvic junction obstruction by intravenous urography. *Top row*: Preoperative ^{99m}Tc-MAG3 study reveals lack of spontaneous drainage from the left kidney. However, there was rapid washout of tracer following diuretic challenge with a washout half-time ($t_{1/2}$) of 2 min and a 30-min residual of 7 %. *Bottom row*: ^{99m}Tc-MAG3 study 3 months after left pyeloplasty. Differential renal function is stable with improved spontaneous drainage from the maturing right kidney. The diuretic phase is unchanged from the preoperative study. Ultrasonography and intravenous urogram revealed mild postoperative improvement

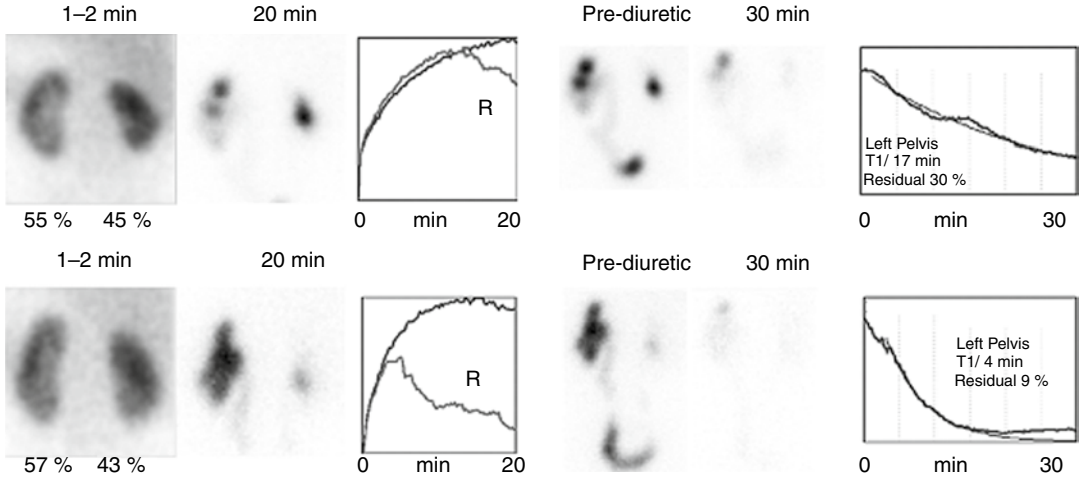

Fig. 12.22 A 1-month-old girl with prenatal diagnosis of left hydronephrosis and no treatment. *Top row*: ^{99m}Tc-MAG3 study shows lack of significant spontaneous drainage from the left kidney. The washout half-time is 17 min with a 30-min residual of 30 %. *Bottom row*: Approximately 1 year later, there is an improvement in spontaneous drainage from the left kidney, a post-diuretic washout half-time of 4 min, and a 30-min residual of 9 %

The apparent function of the hydronephrotic kidney will be affected by the severity of urinary obstruction. High pressure in the pelvicaliceal system can result in reduced renal blood flow and decreased cortical function. In the young, this can be reversed after relief of the urinary obstruction. A more accurate assessment of renal function can be attained after the obstruction is relieved (Fig. 12.25) [67, 68].

The amount of tracer uptake in the renal parenchyma is directly related to the functional capacity of the kidney. Renal blood flow decreases rapidly with increased pressure in the pelvicaliceal system (Fig. 12.3). This can be reversible for

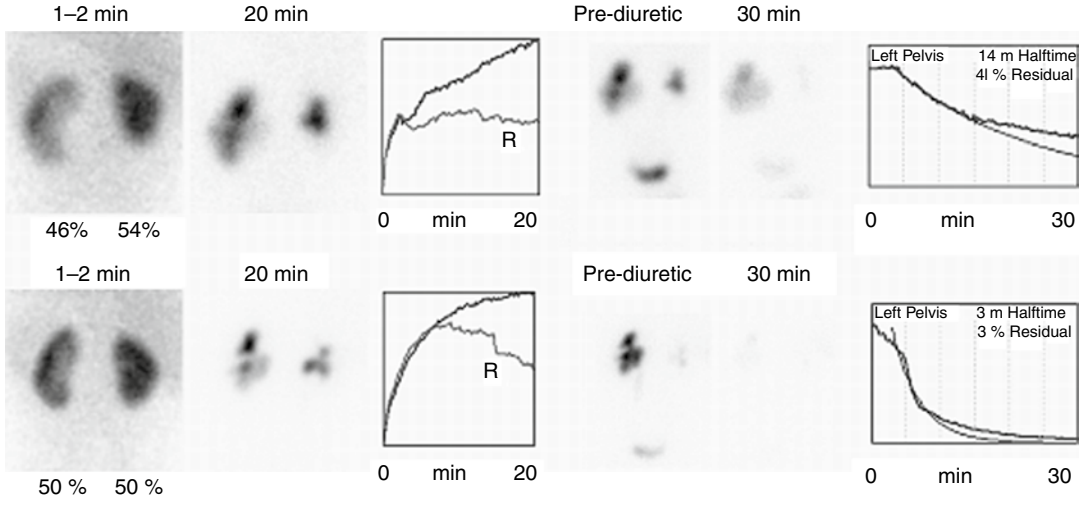

Fig. 12.23 A 2-month-old boy with congenital left hydronephrosis ^{99m}Tc-MAG3 study. *Top row*: Lack of significant spontaneous drainage from the left kidney. Following diuretic challenge, there was a washout halftime of 14 min with a high (41 %) 30-min residual. *Bottom row*: Following left pyeloplasty, there is an improvement on the split renal function to 50 % and a rapid washout following diuretic challenge ($t_{1/2}$ = 3 min, 30-min residual = 3 %)

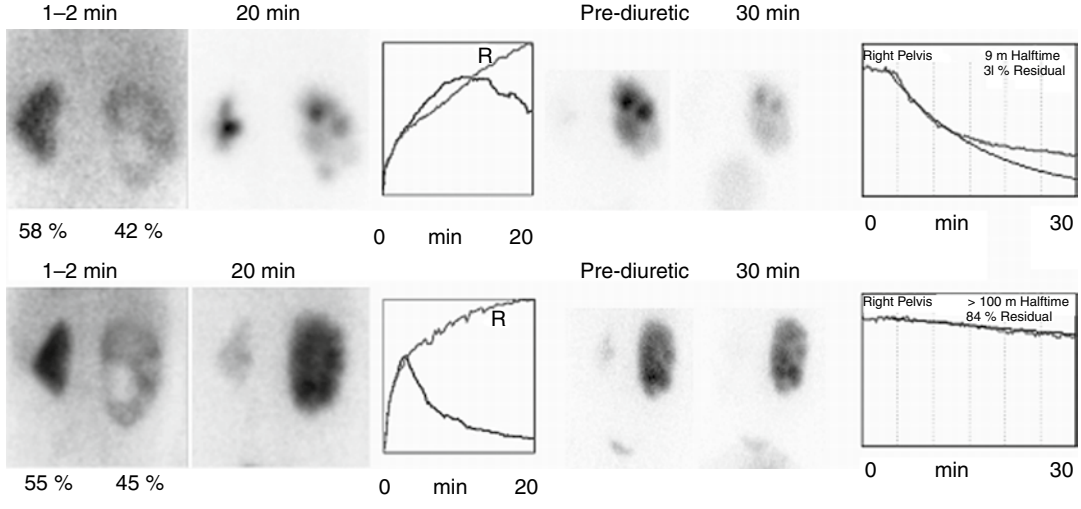

Fig. 12.24 Worsening ureteropelvic junction obstruction. A 6-month-old boy with prenatal diagnosis of right hydronephrosis. *Top row*: Baseline ^{99m}Tc-MAG3 study showing right hydronephrosis, lack of spontaneous drainage from the right kidney, and washout following diuretic challenge (washout $t_{1/2}$ = 9 min and 31 % residual). *Bottom row*: 6 months later, there is no significant spontaneous drainage from the right kidney and the diuretic renogram is grossly abnormal ($t_{1/2}$ > 100 min with a 30-min residual of 84 %). There is an apparent slight increase in right renal function. The patient underwent right pyeloplasty to relieve the obstruction

a period of time, but if increased pressure is persistent, reduction in blood flow and function can become permanent. In studies of hydronephrosis due to obstruction, the obstructed kidney may take up more tracer than the contralateral side. It has been thought that the stressed, obstructed kidney develops transiently increased blood flow.

Over time, renal function in an obstructed kidney will be reduced. It has been suggested that in preoperative patients in whom the cortical

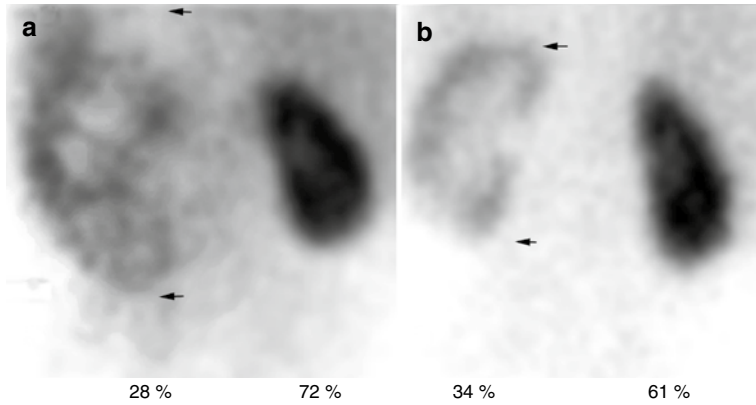

Fig. 12.25 Left ureteropelvic junction obstruction, preoperative and postoperative ^{99m}Tc-MAG3 parenchymal phase images. A 2-year-old patient with left ureteropelvic junction obstruction, before and after left pyeloplasty. (**a**) The preoperative image reveals a large left kidney with low cortical uptake and severe pelvicaliectasis. The cortical transit time of the tracer was prolonged. (**b**) The postoperative study shows a smaller left kidney with improved tracer uptake and normal cortical transit time. *Arrows* indicate upper and lower limits of the left kidney

time-activity curves appear more nearly normal than the total kidney curve, there is a strong likelihood of improvement after the obstruction is relieved. Conversely, abnormal cortical curves may be associated with a poor prognosis for functional improvement [69]. It usually is possible to identify a single site of obstruction at the ureterovesical or the pelvicaliceal junction, but obstruction at both the pelvicaliceal and ureterovesical junctions may be difficult to detect. Detection of the level of obstruction depends on adequate renal function and the presence or absence of dilatation of the pelvicaliceal system and ureter [70]. Differentiating obstructed from dilated nonobstructed systems can be achieved by serial imaging after intravenous administration of furosemide (diuretic renography).

Pyelonephritis

Clinical Features

Urinary tract infection (UTI) is a common problem in children. Presenting signs and symptoms of children with UTI are varied and sometimes confusing. Infection may be confined to the bladder (cystitis); it may involve the upper collecting systems (ureteritis, pyelitis) or the renal parenchyma (pyelonephritis). This differentiation can be difficult to make on clinical grounds alone [71]. Patients may present with fever, flank pain or tenderness, malaise, irritability, leukocytosis, and bacteriuria, but there may be no clear indication that there is renal parenchymal infection. Occasionally, patients with pyelonephritis may present with fevers of unknown origin, particularly in neonates and infants. Prospective clinical studies have shown that commonly used clinical and laboratory findings are unreliable in differentiating acute pyelonephritis from lower UTI in children [72]. Acute pyelonephritis can result in irreversible renal damage (scarring), which in the long term leads to hypertension and/or chronic renal failure [73]. Experimental and clinical studies have shown that renal scarring can be prevented or reduced by early effective antimicrobial therapy of pyelonephritis [74–76].

Vesicoureteral Reflux and Pyelonephritis

Although the coexistence of vesicoureteral reflux and pyelonephritis is well documented (see Chap. 13), many cases of pyelonephritis occur in the absence of documented vesicoureteral reflux. Once acute pyelonephritis occurs, the subsequent development of renal scarring may be independent of vesicoureteric reflux [39, 77–83]. That is,

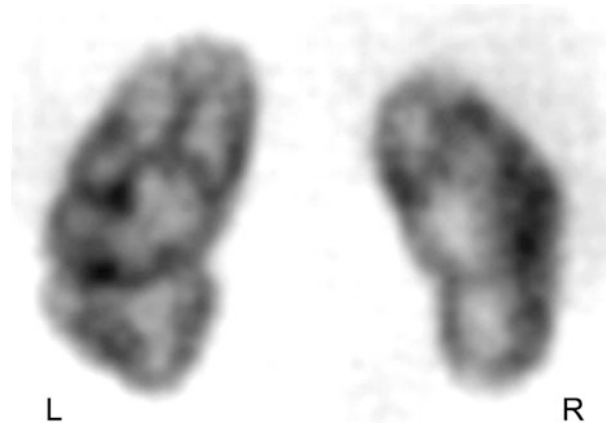

Fig. 12.26 Fetal lobation demonstrated on a ^{99m}Tc-DMSA cortical scan in a 1 month-old infant with vesicoureteral reflux. There is decreased relative function in the right kidney, but no focal cortical defects are identified. Normal fetal lobation is seen in both kidneys

some patients presenting with febrile UTI in the absence of documented vesicoureteral reflux can develop renal scaring. Therefore, it may be prudent to assess renal cortical integrity in all patients with a febrile UTI. It would seem unwise to limit evaluation of cortical integrity in UTI only to those patients who present with a history of vesicoureteral reflux. Diminished ^{99m}Tc-DMSA uptake at the site of acute pyelonephritis probably reflects both tubular dysfunction and focal ischemia related to microvascular changes [93, 94, 95].

Cortical Scintigraphy of Pyelonephritis

Renal cortical scintigraphy with ^{99m}Tc-DMSA can be a reliable, simple, and practical imaging technique for routine use in the initial evaluation and follow-up of children with febrile UTI. It is useful to identify the degree of renal damage and to assess recovery or residual renal damage. The high sensitivity of ^{99m}Tc-DMSA scintigraphy for the early diagnosis and localization of acute pyelonephritis is well established [50, 51, 84–86]. The sensitivity of ^{99m}Tc-DMSA scintigraphy for pyelonephritis is 96 % and the specificity is 98 % [87]. Imaging strategies in patients suspected of pyelonephritis or patients with sudden onset of fever, flank pain, and pyuria or bacteriuria should include ^{99m}Tc-DMSA scintigraphy [88–90].

Images should be obtained in the posterior and posterior oblique projections using a parallel-hole, high or ultrahigh-resolution collimator. Pinhole magnification provides greater diagnostic sensitivity than the parallel-hole collimator for the detection of small focal cortical defects. Technetium-99m-DMSA SPECT provides additional sensitivity and specificity over planar imaging in the evaluation of patients suspected of having pyelonephritis (Figs. 12.15 and 12.16) [85, 91, 92].

In normal kidneys, ^{99m}Tc-DMSA scintigraphy shows a pattern of tracer distribution reflecting the morphology of the renal cortex. No tracer uptake is seen in the medulla or in the collecting system. Flattening of the superolateral aspect of the left cortex may be due to splenic impression. Irregularities in the contour of the renal image may be due to fetal lobations (Fig. 12.26). In these instances, cortical thickness and tracer uptake are normal. Acute pyelonephritis usually appears as a single or as multiple focal areas of reduced or absent uptake with a soft edge, without deformity of the renal outline or apparent loss of volume (Figs. 12.27, 12.28, 12.29, and 12.30).

In some cases, reduced uptake may be accompanied by an acute increase in volume of the affected area. Although the majority of lesions occur in the upper or lower poles, the mid-zone is not protected, and cortical defects can be seen in this area, also. By comparison, renal scars typically show loss of cortical volume with relatively sharp edges to the cortical defect. A less common scintigraphic pattern is one of diffusely decreased tracer uptake throughout an enlarged kidney. If treated appropriately within 48 hours, acute

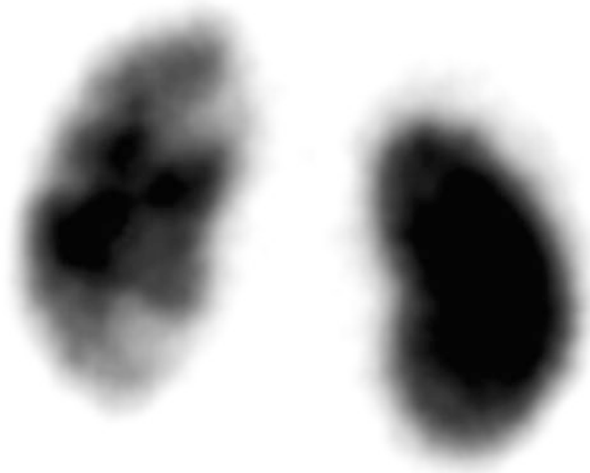

Fig. 12.27 Acute multifocal pyelonephritis in a 2-year-old boy who presented with recurrent fever and left flank pain. The patient had no documented vesicoureteric reflux. ^{99m}Tc-DMSA planar scintigraphy reveals several cortical defects in the left kidney

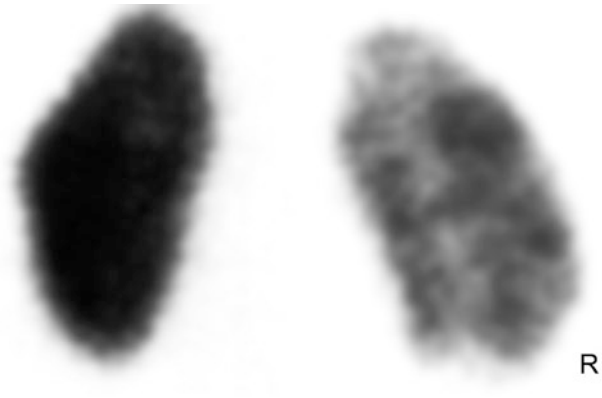

Fig. 12.28 Diffuse acute pyelonephritis. Diffuse and focal pattern of decreased ^{99m}Tc-DMSA uptake in an enlarged (swollen) right kidney

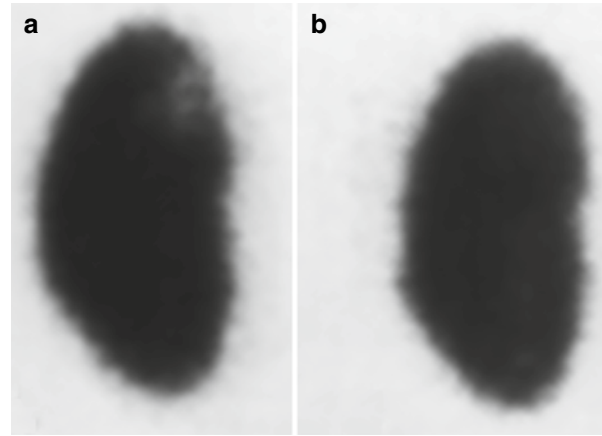

Fig. 12.29 Resolution of acute pyelonephritis. (**a**) Magnified image of a 3-month-old infant at the time of acute febrile urinary tract infection shows focal decreased uptake of ^{99m}Tc-DMSA in the medial aspect of the left upper pole. (**b**) Corresponding image 6 months later shows complete resolution

pyelonephritis may resolve completely and scintigraphic images typically would become normal within 4–6 months (Fig. 12.31).

Alternatively, without adequate and early antibiotic treatment, a permanent cortical scar may develop. A mature cortical scar is usually associated with contraction and apparent loss of volume of the involved cortex. This may manifest as cortical thinning, flattening of the renal contour, or a wedge-shaped defect. The

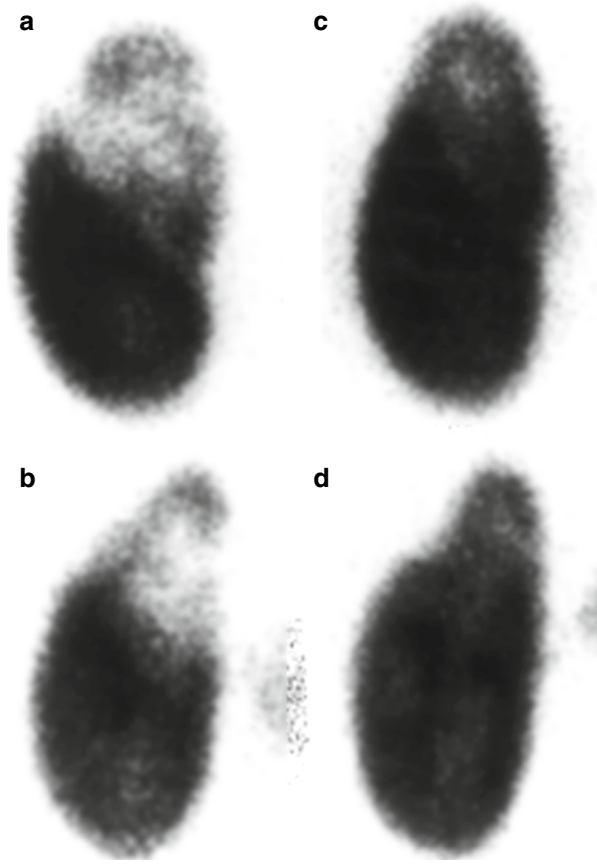

Fig. 12.30 Progression of acute pyelonephritis to cortical scar. Posterior (**a**) and posterior oblique (**b**) images of the left kidney from a 5-year-old child at the time of acute febrile urinary tract infection demonstrate focally decreased ^{99m}Tc-DMSA uptake in the upper pole with preserved renal outline and without evidence of volume loss. Corresponding images obtained 1 year later (**c**, **d**) show contraction and apparent loss of volume of the upper pole, consistent with cortical scarring

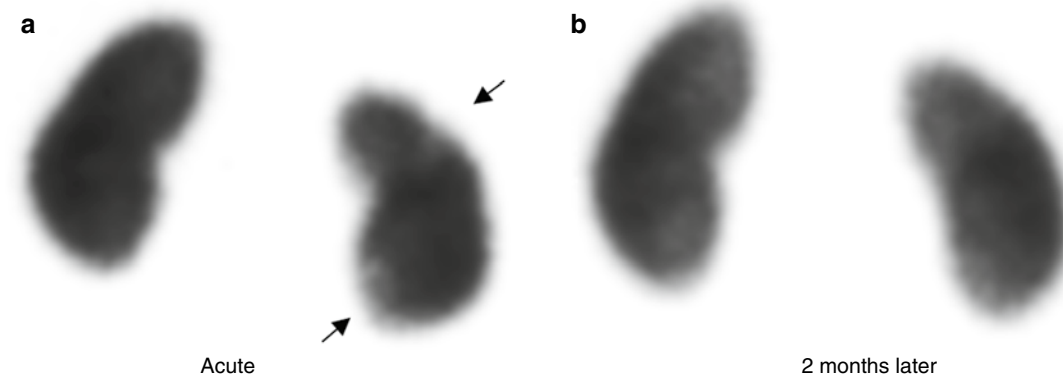

Fig. 12.31 Recovery of cortical function with rapid antibiotic therapy of a febrile urinary tract infection. The 9-year-old girl presented with right flank pain and fever. A urinary infection was diagnosed. (**a**) ^{99m}Tc-DMSA demonstrates focal cortical defects (*arrows*) in the right kidney. Ultrasonography was normal. (**b**) Two months later, a follow-up ^{99m}Tc-DMSA cortical renal scan shows complete resolution of cortical defects. With rapid antibiotic therapy of pyelonephritis, cortical scarring can be avoided

scintigraphic pattern of a maturing scar varies according to the severity, age, and location of the lesion as well as the rate of growth of surrounding normal tissue.

The diminished uptake of ^{99m}Tc-DMSA in areas of acute inflammation probably reflects both focal tubular cell dysfunction and ischemia [81, 93, 94, 95].

Intravenous Urography and Renal Ultrasonography

The limited sensitivities of intravenous urography and ultrasonography for identifying early renal infection have been well-studied [87, 88, 96–98]. Ultrasonography is very useful in diagnosing renal or perirenal abscesses, but less valuable in acute pyelonephritis in which renal enlargement may be the only abnormal finding. Intravenous urograms are abnormal in only 24–26 % of patients with acute pyelonephritis [96, 98]. Possible abnormal urographic findings include a renal pelvis of small volume, dilated and distorted pelvicaliceal structures, renal enlargement, delayed pyelogram, reduced concentration of urographic material, and dilatation of the ureter without obstruction. In contrast to urography, cortical scintigraphy can detect cortical defects that do not deform the renal outline or the collecting system [97, 99]. Computed tomography is an effective technique for documenting the nature of parenchymal involvement, particularly for the evaluation of the perinephric space. Concern about CT radiation exposures limits its use; therefore, routine use in the initial and follow-up evaluation of children with UTI is not practical, and CT should be reserved for complicated cases [100, 101]. The role of magnetic resonance imaging (MRI) in the diagnosis of acute pyelonephritis remains to be defined [102].

In the diagnosis of pyelonephritis, the combination of ultrasonography and cortical scintigraphy is useful. Changes secondary to pyelonephritis may be recognized on ultrasonography as hyperechoic or hypoechoic foci, loss of corticomedullary differentiation, focal or diffuse renal enlargement, and mild or moderate dilatation of the renal pelvis. However, renal ultrasonography has proved to have a low sensitivity for the detection of acute focal inflammatory changes of the renal cortex. In a prospective study, ultrasonographic changes consistent with acute pyelonephritis were found in only 39 % of the children with scintigraphically documented acute pyelonephritis. When abnormal, ultrasonography underestimated the number and extent of the pyelonephritic lesions [77]. Ultrasonography should not, therefore, be regarded as the primary imaging technique for the diagnosis of acute pyelonephritis. Ultrasonography is, however, highly reliable for the detection of hydronephrosis and of the congenital abnormalities that may be associated with UTI in some patients.

Renal Vein Thrombosis

Most types of acquired renal disease in newborns are due to circulatory disturbances, such as renal arterial or venous thrombosis. Approximately two-thirds of all cases of renal vein thrombosis occur in the pediatric age group, with most seen during the neonatal period. In older children, renal vein thrombosis may develop as a consequence of nephrotic syndrome or severe illness. Nephrotic syndrome is a very frequent cause of large-vessel thrombosis because of urinary losses of antithrombin III, protein C, protein S, and other factors. In infants renal vein thrombosis usually is related to venous stasis secondary to shock, septicemia, or dehydration. The diagnosis of renal vein thrombosis may be suggested by the presence of oliguria, mild hematuria, and proteinuria. Renal vein thrombosis also is seen in infants of diabetic mothers and children with congenital heart disease. Consumptive coagulopathy or intravascular coagulation may be present in some of these patients [78, 103–109].

Renal vein thrombosis has been described as a bilateral disease, with asymmetric involvement. Because of this characteristic, a minor lesion in the apparently noninvolved kidney may be missed. Most frequently, the thrombus originates in the interlobar or arcuate veins and less commonly in the main renal vein. The thrombus may extend into the main renal vein and the inferior vena cava, or in a retrograde fashion, it may involve the renal cortex. The venous obstruction then leads to infarction and hemorrhage. Blood leaking into the interstitium and renal tubules may ultimately result in fibrosis. Most patients with renal vein thrombosis are treated medically with maintenance of normal fluid and electrolyte balance [107].

There is considerable variability in the urographic identification of renal vein thrombosis. In

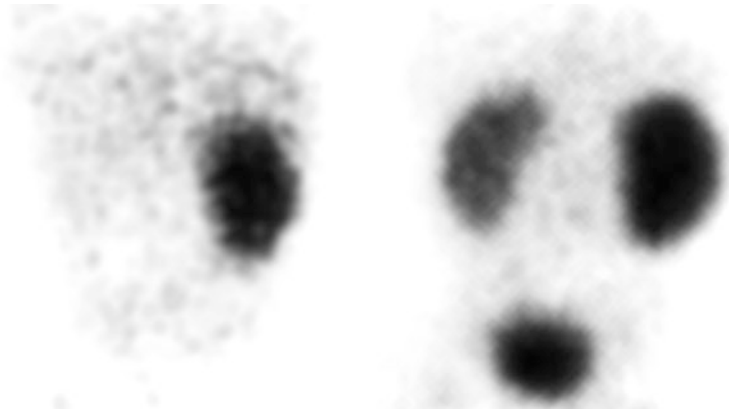

Fig. 12.32 Renal vein thrombosis. This ^{99m}Tc-DMSA study was performed in a premature, 1,400-g female infant who developed hypertension after withdrawal of an umbilical artery catheter. Ultrasonography showed two kidneys of normal size. On the initial study (*left panel*), the kidney is not visualized. After treatment with hydralazine, the patient became normotensive, and another study 3 weeks later showed return of left renal function (*right panel*)

most patients with this condition, the kidney involved is not visualized by intravenous urography. Before modern nuclear medicine techniques were widely employed, it was thought that affected renal units not visible on initial urographic examination virtually ensured an atrophic, functionless kidney later [110]. Doppler ultrasonography typically shows decreased or absent flow in the affected kidney or renal vein.

Renal scintigraphy using ^{99m}Tc-MAG3 or ^{99m}Tc-DMSA is a sensitive method for screening patients with renal vein thrombosis because the findings on serial renal scintigraphy that show the evolution of renal function correlate well with the ultimate outcome [111].

In severe cases, there may be no perfusion or apparent function in the involved side. A follow-up study may be useful to demonstrate the residual renal function after recovery. Radionuclide studies may reveal information of prognostic significance, with a normal study predicting a rapid and complete recovery (Figs. 12.32 and 12.33).

Renal Infarction

Renal infarction can occur in patients with cyanotic congenital heart disease, polycythemia, atrial fibrillation, dehydration, or trauma. Aortic thrombosis and renal infarction are also well-recognized complications of prolonged umbilical artery catheterization. Treatment with thrombolytic agents has produced resolution of the clot and recovery of renal function in some cases. Technetium-99m-DMSA scintigraphy demonstrates focal perfusion defect(s) in the affected kidney(s) (Fig. 12.34).

Hypertension

The prevalance of hypertension in children is less than 2.5 % [112], but the reported prevalance of secondary hypertension varies with the source of patients [113–115]. The younger the patient, the more likely that hypertension has a secondary cause, and the most common cause of secondary hypertension in children is renal disease. Renal disease associated with hypertension can be caused by diseases that involve the renal arteries or the renal parenchyma. In a study of 563 pediatric patients with secondary hypertension, 78 % had a renal abnormality and 12 % were diagnosed with renal artery disease [114]. Less frequently, secondary hypertension may be caused by disorders of the endocrine, cardiovascular, or nervous systems. Radionuclide renal studies play an important role in the evaluation and treatment of hypertension in infants and children.

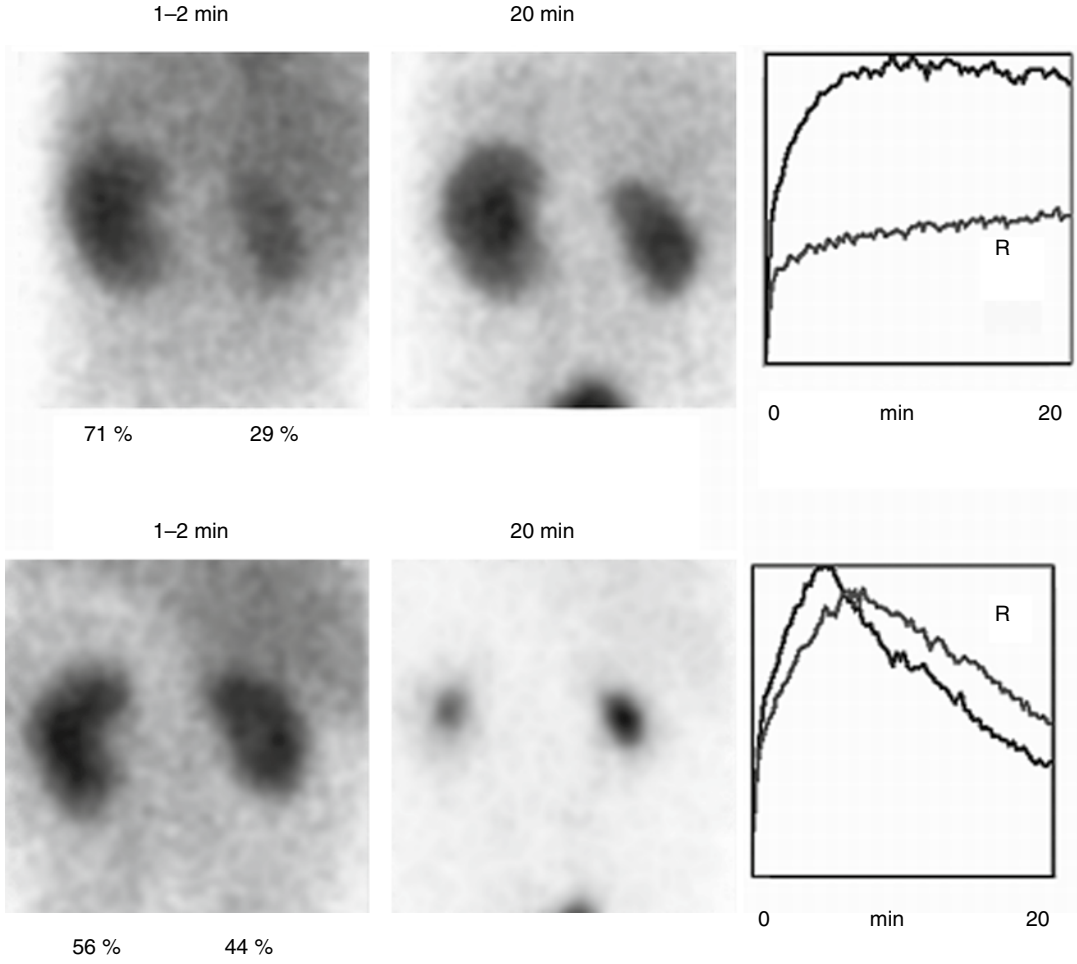

Fig. 12.33 Renal vein thrombosis demonstrated by a ^{99m}Tc-MAG3 renogram in a 1-week-old girl presenting with oliguria, cardiomegaly, and hypertension. *Top row*: First study shows asymmetric renal function (L>R) with bilateral delay in transit time. There is marked cortical retention of tracer. *Bottom row*: 1 month later, there is more symmetric renal function (L=56 %, R=44 %) and a normalization of cortical transit. There is minimally delayed drainage of tracer from the right pelvis. The time activity curve demonstrates a longer time to peak and slower drainage of the collecting system on the right

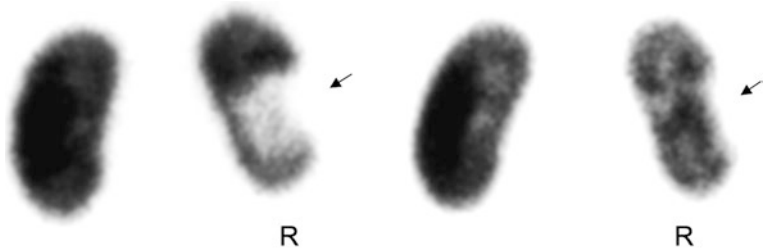

Fig. 12.34 Renal infarct. A 16-year-old boy with cyanotic congenital heart disease had undergone several surgical interventions and presented with acute right flank pain. *Left*: Initial ^{99m}Tc-DMSA scintigraphy shows a well-defined defect in the right kidney due to ischemia. *Right*: A follow-up study 1.5 months later shows considerable resolution of the defect (*arrow*), but there is a persistent scar

Some of the renal causes of hypertension, such as infarction, postpyelonephritic scarring, and posttraumatic lesions, are easily diagnosed by conventional renal scintigraphy. Both dynamic and static renal scintigrapy are very sensitive for the identification of renovascular hypertension [95, 109, 116]. On dynamic scintigraphy, the affected kidney is usually smaller and shows less uptake than the contralateral kidney. With mild renal artery stenosis, a renogram may appear normal. When stenosis is severe, however, excretion of tracer in the collecting system is delayed or even absent during the 20-min observation period. Parenchymal retention of the tracer increases with severity of stenosis. Technetium-99m-DMSA scintigraphy in patients with renovascular hypertension typically reveals renal asymmetry; the affected kidney is smaller, has decreased relative function, and may demontrate cortical defects.

A kidney with a stenotic artery may remain adequately perfused due to the renal autoregulation mechanism. The radionuclide renal study therefore may appear normal in many patients with renal artery stenosis. The efficacy of renal scintigraphy for the diagnosis of renovascular hypertension, however, can be improved by the use of angiotensin-converting enzyme (ACE) inhibitors, such as captopril. These block the formation of angiotensin II, resulting in dilatation of the efferent arterioles and a decrease in the transcapillary pressure gradient. This can lead to a marked decrease in glomerular filtration in a kidney with significant renal artery stenosis. This stimulated loss of renal function can be detected by renal scintigraphy and renography [117–121].

The choices of radiopharmaceutical, ACE inhibitor, and examination technique vary among institutions. In the original studies in pediatric patients, ^{99m}Tc-DTPA was used [118]. Subsequent experience has shown that either glomerular or tubular agents can be used. Technetium-99m-MAG3 captopril renography appears to be effective. The radiopharmaceutical of choice for detecting focal parenchymal abnormalities such as infarcts and pyelonephritic scars is ^{99m}Tc-DMSA [52, 88, 116, 122]. Administration of captopril may cause a decrease in the renal ^{99m}Tc-DMSA uptake in patients with renovascular hypertension [123].

Either captopril (1 mg/kg, up to 50 mg) or enalaprilat can be used as the ACE inhibitor. To ensure better absorption of captopril, the patient should not eat solids for approximately 4 h before the study. The advantage of enalaprilat is that it is administered intravenously and, unlike oral captopril, its effect does not depend on variable rate of absorption through the gastrointestinal tract.

A significant fall in blood pressure can be observed even after a single dose of captopril. Therefore, the patient should be well hydrated, well monitored, and an intravenous access maintained throughout the study. The blood pressure should be monitored every 5–15 min. The probability of severe hypotensive crisis is even higher with intravenous enalaprilat, so that its routine use is not recommended. Diuretics may exaggerate the hypotensive effect of ACE inhibitors and should not be used in conjunction with captopril renography.

Ideally, both a baseline and stimulated study should be performed. An alternative approach is to obtain the initial study with an ACE inhibitor and then, if the first study is abnormal, repeat the study without the use of ACE inhibitor.

The scintigraphic manifestations of decreased renal function induced by ACE inhibition in the presence of hemodynamically significant renal artery stenosis depend on which radiopharmaceutical is used. The primary effect of ACE inhibitors is decreased GFR. Therefore, the effect of an ACE inhibitor on a ^{99m}Tc-DTPA study will be observed as a varying degree of decreased extraction of tracer and delayed visualization of the collecting system, whereas with the use of tubular agents, prolonged cortical retention of the tracer is seen. Therefore, detection of focal cortical changes is easier with ^{99m}Tc-MAG3 (Figs. 12.35a–c and 12.36).

The typical findings of a positive captopril study include an decrease in the differential renal uptake, an increase in cortical transit time, a prolongation of time to peak, and retention of tracer in the renal parenchyma. Scintigraphic abnormalities in unilateral renal artery stenosis can be appreciated visually by inspection of the images and the renal time-activity curves. Numerical or

semiquantitative evaluation of time-activity curves has been utilized. In the presence of bilateral renal artery stenosis, narrowing is usually asymmetrical, as is the effect of captopril on each kidney. In this case, evaluation of the time-activity curves may be most revealing.

In hypertensive adult patients, scintigraphic abnormalities induced by the administration of captopril appear to be strongly associated with cure or improvement in blood pressure control following revascularization or nephrectomy. Cases in which captopril does not induce scintigraphic changes are associated with failure of revascularization or nephrectomy [124–127]. Such failure may be due to a high prevalence of coexisting essential hypertension. Angiographic demonstration of renal artery narrowing in older patients does not, therefore, necessarily indicate renovascular hypertension, and revascularization may fail to cure hypertension. In hypertensive children, however, a negative captopril renogram rarely is associated with angiographic evidence of renal artery stenosis.

Congenital Anomalies

Ectopic Kidney and Solitary Kidney

One or both kidneys may be displaced in association with, or independent of, other renal malformations. Ectopic kidneys situated in the pelvis may be difficult to visualize on intravenous urography, partly because of interference by surrounding bony structures. Scintigraphy with ^{99m}Tc-DMSA or ^{99m}Tc-MAG3 is helpful for diagnosing renal ectopia or a solitary kidney (Figs. 12.6 and 12.37).

Horseshoe Kidney

With horseshoe-shaped kidneys, fusion is between the two lower poles. Radionuclide studies are useful for assessing functional abnormalities when there are symptoms referable

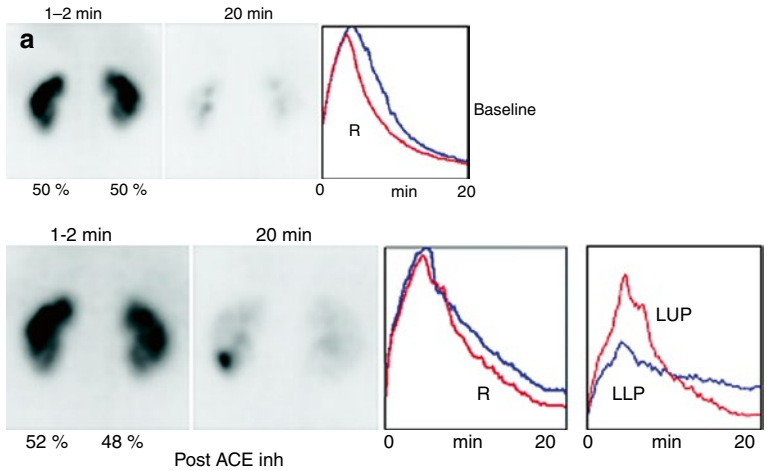

Fig. 12.35 (**a**) Hypertension. Baseline and post-angiotensin-converting enzyme (*ACE*) inhibitor ^{99m}Tc-MAG3 studies. On the baseline study (*top*), renal function is symmetric, and there is no retention of tracer in the renal parenchyma. The time activity curve shows a slightly delayed time to peak in the left kidney. On the post-ACE inhibitor study (*bottom*), relative renal function appears normal. However, there is focal parenchymal retention of tracer in the left lower pole. The time-activity curve of the left lower pole (*LLP*) shows lower peak amplitude and higher residual at 20 min than the left upper pole (*LUP*). (**b**) Baseline study (*top*): 1- to 2-min and 20-min images of the left kidney reveal normal intrarenal distribution of tracer. Similar images of the left kidney (*bottom*) after administration of ACE inhibitor reveal decreased tracer uptake in the left lower pole (1–2 min) and focal parenchymal tracer retention in the same region after 20 min. (**c**) Renal angiography reveals arterial stenosis to the involved segment of the left lower pole. Following selective balloon angioplasty, the patient's blood pressure dropped from 170/110 to 120/60 mmHg

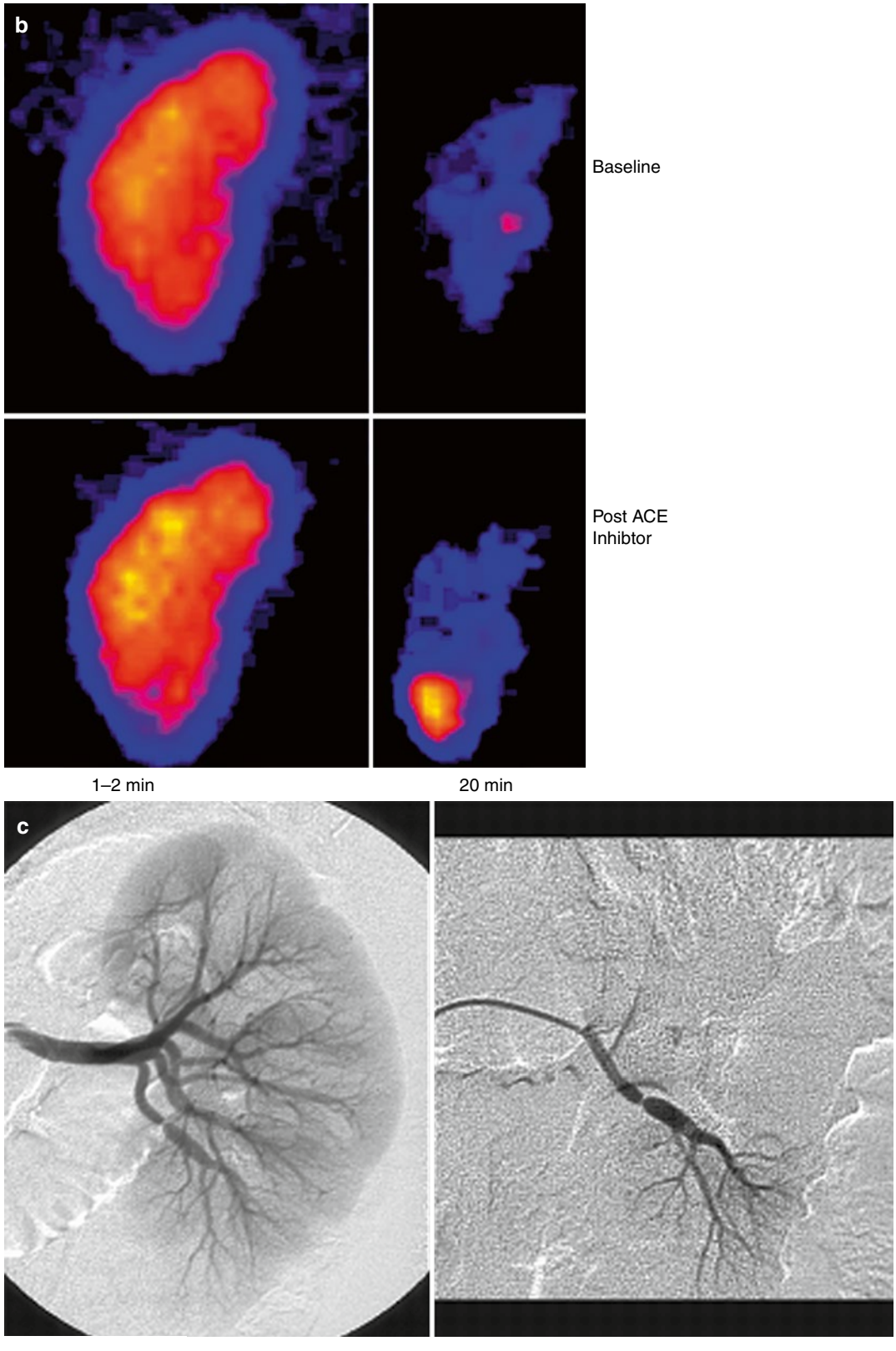

Fig. 12.35 (continued)

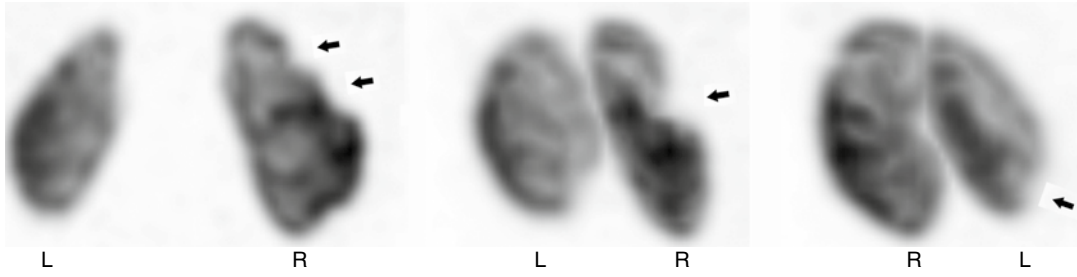

Fig. 12.36 Patient with renovascular hypertension and DMSA SPECT revealing well-defined cortical defects caused by renal artery stenosis. *Arrows* show well-defined cortical defects in the right kidney

Fig. 12.37 Ectopic right kidney. ^{99m}Tc-DMSA renal scan of a 2.5-month-old female showing an ectopic right kidney in the right flank and pelvis

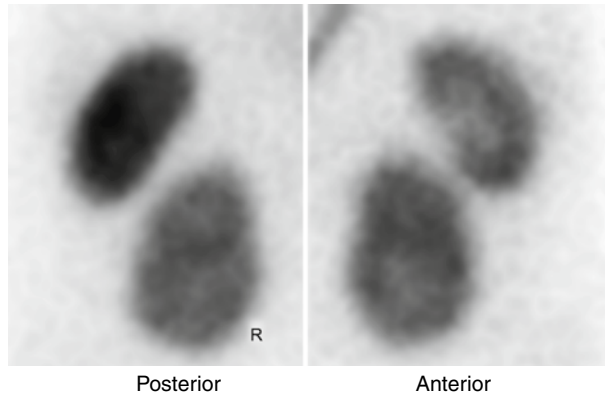

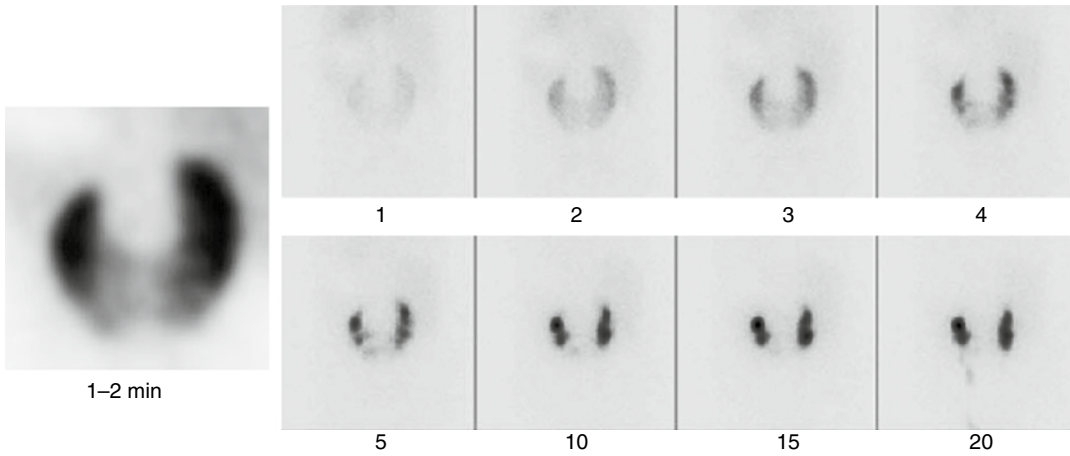

Fig. 12.38 Horseshoe-shaped kidney imaged with ^{99m}Tc-MAG3 dynamic renography

to the kidney, such as infection, hypertension, and hematuria. Technetium-99m-DMSA images (including anterior views) show whether the kidneys are joined by functioning renal tissue or by a fibrous band (Fig. 12.38).

Duplication

Duplication of the ureter and renal pelvis is one of the most common abnormalities of the urinary tract. It occurs bilaterally in 25–30 % of affected patients. The upper pole ureter tends to insert

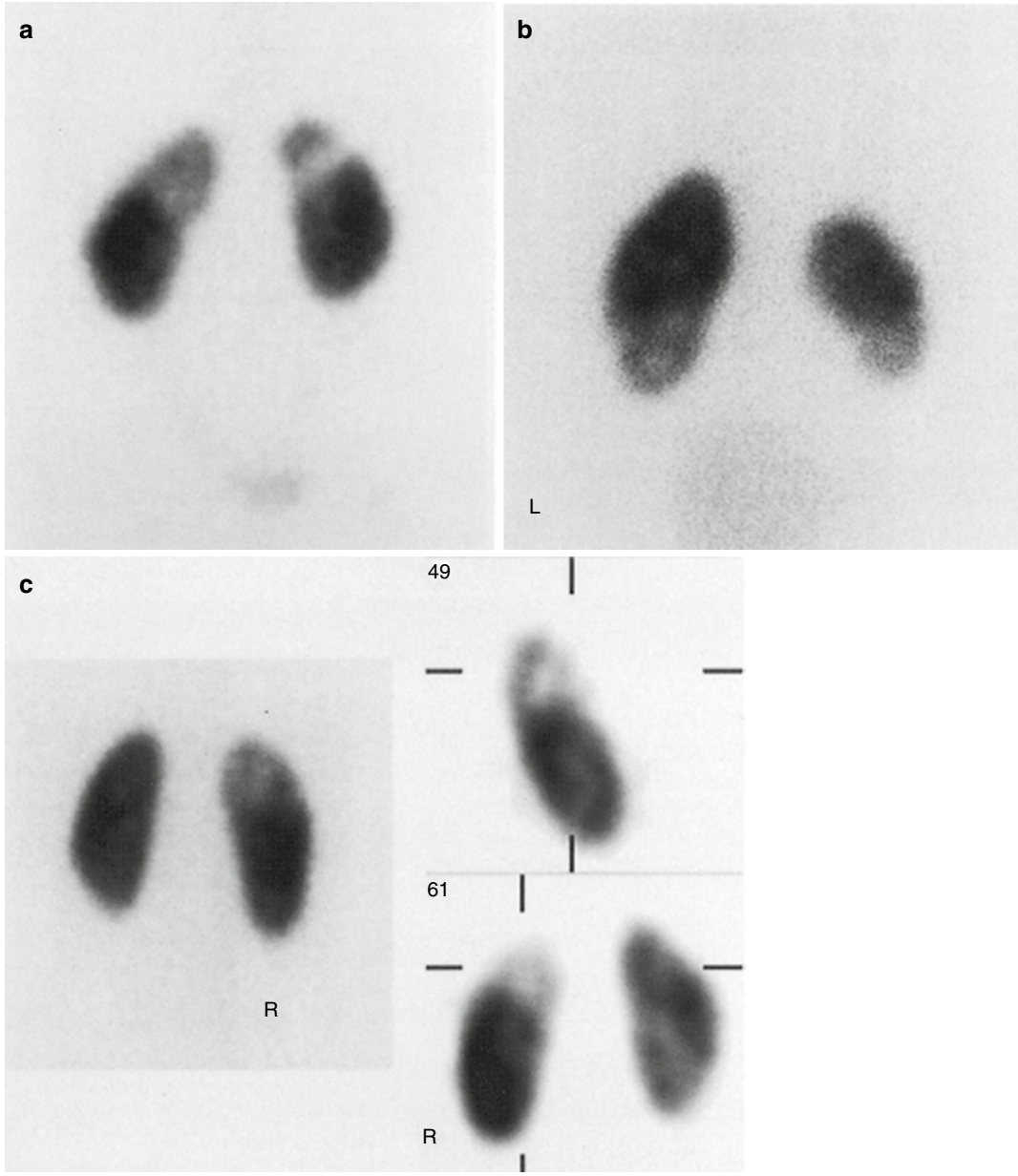

Fig. 12.39 Renal duplication. Three examples of ^{99m}Tc-DMSA scintigraphy in kidneys with duplication. (**a**) Bilateral duplication with relatively poor function in both upper moieties. (**b**) Bilateral duplication with less function in the smaller right kidney and in both lower moieties. (**c**) Conventional planar scintigraphy (*left*) and selected sagittal and transverse SPECT slices (*right*) in unilateral duplication with relatively poor function of the right upper moiety, anteriorly

more caudally and medially than the normally placed lower pole ureter. The ureter from the lower pole is more often affected by vesicoureteral reflux, whereas the upper ureter is more often obstructed. When surgery is contemplated, ^{99m}Tc-DMSA can be used to evaluate the relative function of the upper and lower renal moieties (Figs. 12.12 and 12.39).

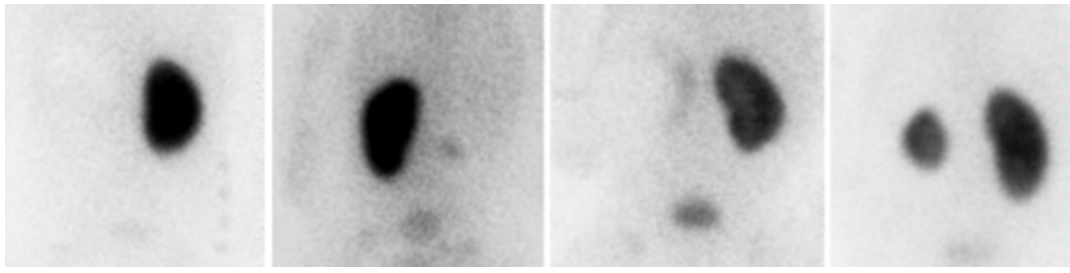

Fig. 12.40 Multicystic dysplastic kidneys (MCDK) imaged with ^{99m}Tc-DMSA scintigraphy. Different appearances illustrating the degree of severity. *0* no evidence of tracer uptake, *1* minimal tracer uptake detected after image enhancement, *2* minimal uptake without image enhancement, *3* substantial uptake in a small kidney

Polycystic Kidney Disease

There are two types of polycystic kidney disease. Autosomal dominant polycystic kidney disease is the more common type, but usually does not present until adulthood. Autosomal recessive polycystic kidney disease usually presents during infancy and is an inherited cystic disorder affecting both kidneys. It is twice as frequent in male infants as in female infants. Scintigraphy with ^{99m}Tc-DMSA often reveals large renal silhouettes and outlines of renal parenchymal uptake surrounding the cysts. The appearance of the scan in polycystic kidney disease depends on the degree of renal involvement. In more severe cases, no functional cortex may be identified by ^{99m}Tc-DMSA.

Multicystic Dysplastic Kidneys

Multicystic dysplasia of the kidney (MCDK) is the most frequent cystic disorder of infants and children [128]. There is marked variation in the size of the lesions and extent of involvement. Classically, MCDK has been described as a mass of noncommunicating cysts with no discernible renal parenchyma or pelvis [129, 130]. Urogenital abnormalities are frequently associated with MCDK. In approximately 75 % of the cases, scintigraphy with ^{99m}Tc-DMSA does not demonstrate tracer uptake in the involved kidney. In some instances, however, some tracer uptake can be seen in small regions of distorted renal parenchyma. Sometimes scintigraphic images of newborns with MCDK will appear similar to the images seen with hydronephrosis (Fig. 12.40).

Prune-Belly Syndrome

Prune-belly syndrome occurs in male infants and manifests as dilatation of the urinary bladder and ureters with a bizarre, wrinkled, flabby abdominal wall [131–134]. The cause of the abdominal muscular deficiency is not known. The most severely affected patients die soon after birth or may be stillborn. Abnormalities associated with this syndrome include pulmonary hypoplasia, renal dysplasia, urethral obstruction, weak chest wall muscles, vesicoureteric reflux, and undescended testes. Dynamic renal scintigraphy reveals a spectrum of findings. Scintigraphy may show dilatation of the pelvicaliceal systems without obstruction; yet others reveal dilatation with apparent obstruction. Technetium-99m-DMSA scintigraphy can help assess regional distribution of functioning renal parenchyma, detect renal scarring, and evaluate the course of the renal disease. Frequently, ^{99m}Tc-DMSA imaging may be delayed until 24 h to allow drainage of the tracer activity from the dilated ureters.

Renal Trauma

Radionuclide imaging is used infrequently in these patients. In some cases, ^{99m}Tc-DMSA scintigraphy can be helpful for detecting nonobvious functional or structural damage to the kidney. Renal scintigraphy can be used to assess recovery or residual damage. Studies using ^{99m}Tc-MAG3 or ^{99m}Tc-DTPA can effectively detect urinary leaks following trauma (Figs. 12.41 and 12.42).

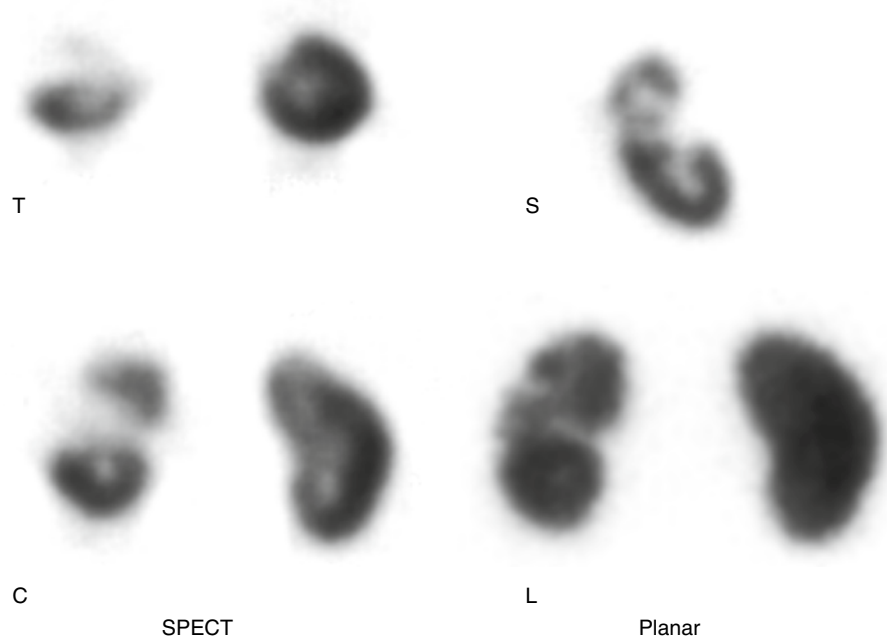

Fig. 12.41 Trauma. Selected transverse, sagittal, and coronal ^{99m}Tc-DMSA SPECT slices as well as planar scintigraphy reveal cortical damage of the left kidney after trauma. These images are from a follow-up study to assess recovery. *T* Transverse; *C* Coronal; *S* sagittal; *L* Left

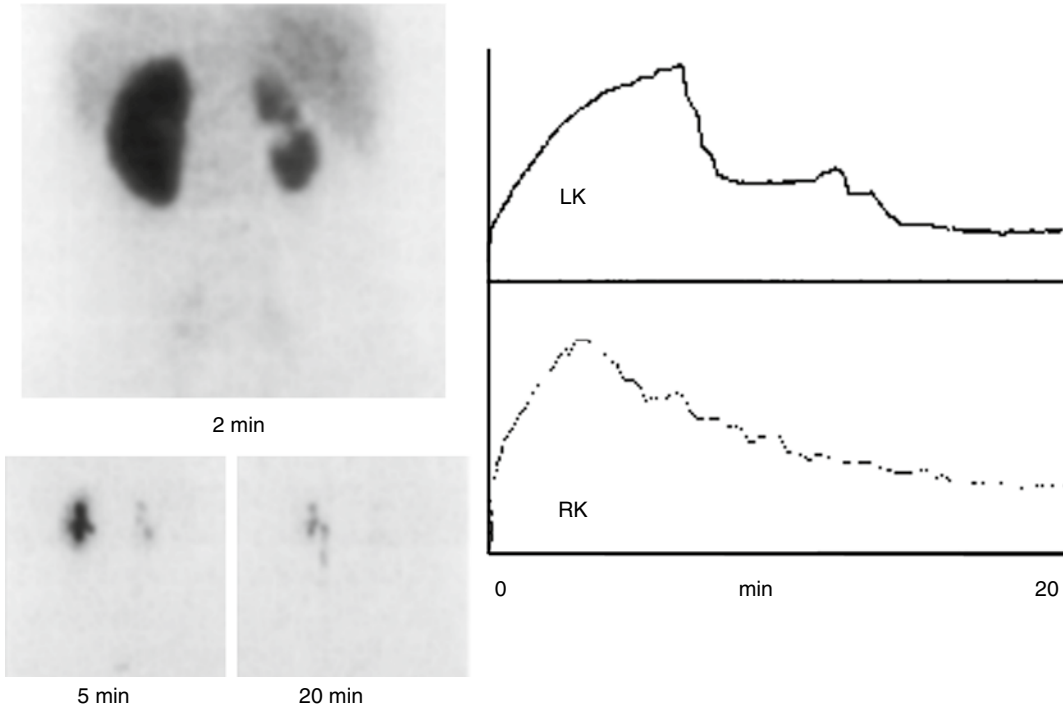

Fig. 12.42 Trauma. Example of a ^{99m}Tc-MAG3 study from a patient who had sustained previous renal trauma. The parenchymal phase (*top left*) reveals a hypertrophic left kidney and a small right kidney with a cortical defect in its midportion at the site of prior traumatic injury. Cortical transit time and drainage are normal bilaterally. *LK* left Kidney; *RK* Right Kidney

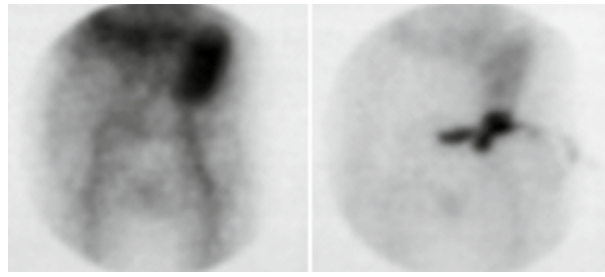

Fig. 12.43 Urinary leak. Postoperatively, this recipient of a renal transplant developed a urinary leak. Selected images of a ^{99m}Tc-MAG3 study (left to right: 2, 20 min) reveal an abnormal accumulation of radiotracer inferior to the left-sided transplant, which corresponded to a urine leak through the transplanted ureter

Acute Renal Failure

With acute renal failure, dynamic renography with ^{99m}Tc-MAG3 will show delayed cortical clearance of tracer. Cortical transit of tracer and appearance of tracer in the renal collecting system is delayed. The typical finding is cortical retention of tracer, but with severe renal insufficiency or renal damage, there may be absent or significantly diminished cortical uptake of tracer. Improvements in function detected on such studies usually precede biochemical changes by 1–2 days. In patients with known urinary obstruction, dynamic renography may be used to exclude concurrent parenchymal disease as a cause of acute renal failure.

Tumors

Renal scintigraphy is very infrequently used in the investigation of renal tumors. Diagnosis and further evaluation of renal and perirenal masses and tumors are carried out with ultrasonography, MRI, and CT. Hypertrophy of a renal column of Bertin may appear as a mass that at times is difficult to distinguish from neoplasm or cyst on urography. Cortical radionuclide imaging can firmly establish the diagnosis of normal renal cortex and absence of tumor [135–137].

Effect of Radiotherapy

Radiation therapy can cause transient or permanent functional defect(s) in the irradiated kidney. This effect can be seen as one or more regions in the kidney with reduced to absent uptake of ^{99m}Tc-DMSA and ^{99m}Tc-MAG3. Prior radiation therapy also can cause cortical retention of ^{99m}Tc-MAG3. Radiation therapy can cause delayed uptake and retention of dynamic renal tracers.

Renal Transplantation

Living Renal Donors

Living donors comprise approximately 60 % of all donors for renal transplants in children [3]. Renal scintigraphy is useful for assessing both renal function and anatomy in living donors. For example, if previously undetected renal abnormalities are seen, a donor may be considered unsuitable. If a radionuclide study on a living donor reveals renal function asymmetry, the surgeon may elect to transplant the kidney showing less function.

Recipients of Renal Transplants

Radionuclide studies are useful during the early and late periods after renal transplantation to assess surgical results and detect complications [138–144]. As radiopharmaceuticals produce no osmotic load and no pharmacologic effects they can be used safely even in the presence of severe renal transplant dysfunction. It is possible with scintigraphic methods to assess perfusion of the transplant during the early and late postoperative periods and assist in the differential diagnosis of diminished graft function, which includes rejection, obstruction, and urinary leak (Fig. 12.43).

If there are no suspected surgical complications, a baseline evaluation of the transplant is often obtained during the first 24 h following transplantation. Subsequent studies are performed depending on the patient's progress. Renal transplants from living donors that have had short periods of

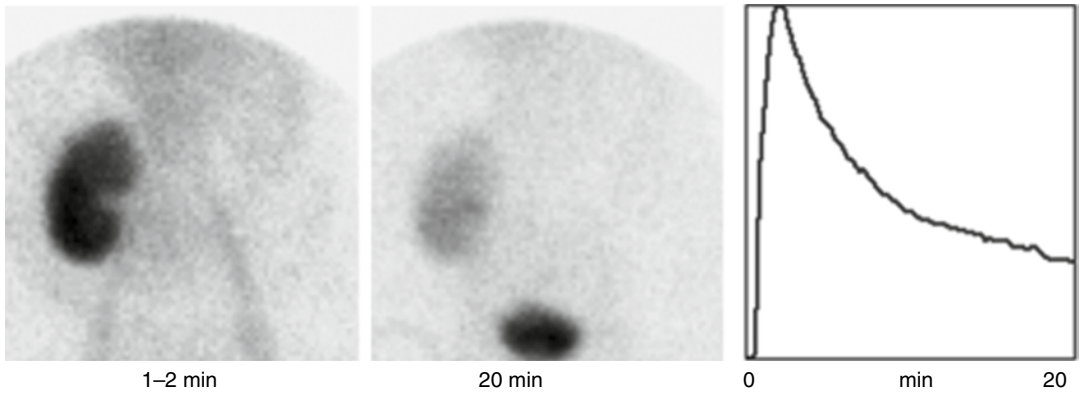

Fig. 12.44 Kidney from a living donor. The recipient was imaged with ^{99m}Tc-MAG3 renography a few hours post-transplantation. Tracer uptake is brisk at 1–2 min, and there is minimal parenchymal or urinary retention at 20 min. The renal time-activity curve shows a time to peak of only 2 min and less than 35 % residual at 20 min. Therefore, there is little post-transplant ATN

cold and warm ischemia often will function immediately after transplantation. The initial uptake of the tracers in these transplants is normal and occasionally more intense than in a normally functioning kidney. In addition, the intrarenal transit time is normal or even faster than normal (Fig. 12.44). After a few days, in the absence of complications, the handling of tracers by the transplant becomes nearly identical to that of normal kidneys.

As many as one-third of grafts, particularly those from deceased donors, are affected by acute tubular necrosis (ATN), which can persist for just a few days or for as long as 2 months after the transplant procedure. In patients with ATN, delayed images obtained with ^{99m}Tc-MAG3 several hours after administration of the tracer reveal retention of the radionuclide within the renal parenchyma with little, if any, accumulation or passage of activity into the renal pelvis, ureter, or bladder. If tracer activity within the transplant is similar to background on radionuclide angiography and later images, it indicates severe depression of renal function. However, the kidney should not be assumed nonviable, as most transplanted kidneys will recover from ATN unless rejection or other complications occur.

Thrombosis

Renal graft thrombosis and infarction is the third most frequent cause of graft loss in pediatric renal transplantation [145]. The apparent lack of perfusion of a renal transplant, seen on radionuclide angiography, does not always signify occlusion of the main renal artery leading to the transplant. Lack of blood flow to a transplanted kidney also may be due to hyperacute rejection. Correlative ultrasonography can be helpful to distinguish thrombosis from renal causes of decreased renal perfusion. Renal graft thrombosis in a living-related donor transplant is most frequently seen when the recipient is less than 5 years of age. On the other hand, thrombosis following cadaveric renal transplant is most common when the donor is young usually less than 5 years of age. All these conditions present as a lack of renal blood flow to the transplant on a radionuclide angiogram and failure to visualize the kidney on subsequent serial images. Chances of recovery of renal function in these patients are remote, and unfortunately, surgical removal of the graft may be indicated.

Rejection

The most common cause of renal graft dysfunction during the first several months following transplantation is an acute rejection episode. As many as 25 % of deceased transplants and 15 % of living-related donor transplant recipients have acute rejection episodes during the first year after transplantation. Rejection is often suspected on the basis of nonspecific clinical findings (fever, tenderness over the graft site) or specific clinical findings (decreased urine output, increased serum

urea nitrogen and creatinine). A renal biopsy is frequently obtained to confirm the diagnosis of rejection. Treatment for acute rejection episodes includes high-dose "pulse" corticosteroid treatment or the use of antilymphocyte preparations. Complications associated with these therapies, particularly opportunistic infections, are sometimes severe.

Renal scintigraphy is generally performed during the evaluation of an apparent acute rejection episode. The scintigraphic findings during acute rejection episodes include diminished perfusion of the graft, poor uptake of ^{99m}Tc-MAG3, and, occasionally, increased size of the renal silhouette. There are no specific findings in renal scintigraphy to confirm renal transplant rejection. The major value of the study is to rule out other conditions (e.g., renal obstruction, vascular comprise, or urinary leak) that could cause diminished graft function. These studies are particularly important, as they provide the basis for avoiding unnecessary therapy when processes other than rejection account for the diminished graft function.

Virtually all acute rejection episodes are reversible with treatment. With many episodes, however, return of graft function to prerejection levels may be delayed for up to several weeks, possibly related to renal interstitial edema secondary to the infiltrating lymphocytes and their subsequent destruction. Serial follow-up radionuclide studies may be helpful for assessing the returning renal function, as these studies often predict the recovery of function 24–48 h before the blood chemistry values improve.

Obstruction

Urinary obstruction is a very rare complication following renal transplantation. It can be difficult to diagnose in the presence of depressed renal function, such as occurs in acute tubular necrosis or after a rejection episode. Obstruction soon after surgery may be due to edema and/or inflammation in the region of the ureterovesical junction, which may be temporary. Later, obstruction may be due to external compression, which may be caused by (1) a lymphocele or scarring secondary to previous surgery or (2) internal obstruction, such as that caused by a ureteral stone or stenosis at the ureteral anastomosis site. In most cases, the transplant ureter is implanted directly into the bladder. In some cases, however, the native ureter may be used as a ureterostomy or, by anastomosis, connected directly to the pelvis of the graft. Because the transplant ureter obtains its blood supply only from the graft, the distal ureter may be poorly perfused, which may result in distal ureteral scarring and obstruction. Partial or even total obstruction of a transplant kidney may be relatively asymptomatic, as the graft is not innervated. Diagnosis of partial obstruction is sometimes difficult, and the use of furosemide after injection of the tracer may aid in the diagnosis. In cases of diminished graft function, ^{99m}Tc-MAG3 sometimes can demonstrates urinary obstruction, even in the presence of severe renal failure.

Urinary Leak

Urinary leak usually occurs in the first few months following transplantation. It can occur at the site of anastomosis of the transplant ureter or through necrosis of the distal transplant ureter related to diminished perfusion. The presence of urinary leak is detected with serial scintigraphy, usually as part of a ^{99m}Tc-MAG3 renogram, with greater sensitivity than other methods because of the high contrast of the radiotracer technique [146]. Multiple images at several minutes to several hours after the injection tracer may be necessary to detect urinary leakage. On the series of scintigrams, the leakage appears as a focal or diffuse area of increasing tracer accumulation outside the confines of the transplant, the ureter, or the bladder. In patients with a post-surgical drain in the abdominal cavity, leaked urine may cleared by the drain and little extravasated tracer may be seen in the abdomina cavity. The drain collection container must be imaged to exclude this possibility. Urinoma usually appears as a photon-deficient area on early images (5–10 min) with subsequent tracer accumulates on later images. If the area that is photon-deficient on early images does not concentrate radiotracer on later images, this region may represent a hematoma or a lymphocele (Fig. 12.43).

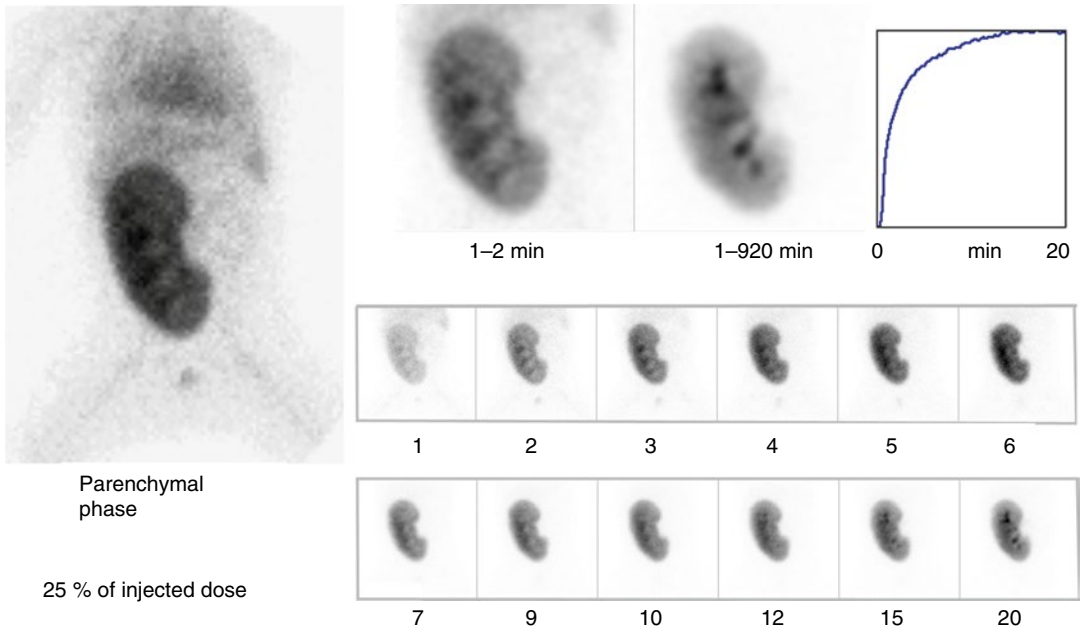

Fig. 12.45 A 9-month-old recipient of a living-related donor kidney transplant who was studied with a ^{99m}Tc-MAG3 renogram 1 day following transplantation. The parenchymal phase reveals a relatively large renal transplant (see the proportion to the baby's whole body). There is prompt and adequate tracer uptake in the viable transplant with delayed transit time and marked cortical retention, consistent with post-transplant ATN. With minimal tracer excretion into the collecting system, no determination can be made about urinary obstruction or leak

Transplantation of Adult Kidneys into Babies

When a kidney from an adult donor is transplanted into a baby, the large disproportion between the size of the transplant and the patient's body may interfere with drainage of the renal collecting system (Fig. 12.45).

Appendix: Quantitative Analysis of Renal Function

Nuclear medicine is unique among medical imaging modalities in that it is capable of providing detailed quantitative physiologic information about the kidneys. In large part, this is due to the availability of radiotracers whose properties approximate those of the classic tracers PAH and inulin.

Although quantitative physiologic information is useful in monitoring patients, producing it in a consistent and accurate way requires close attention to detail. In what follows, we have tried to emphasize the assumptions that are made in some common approaches to the quantitative analysis of the renogram.

Correction for Tissue Attenuation and Detection of Extrarenal Activity

In quantitative analysis of dynamic renal scintigraphy, one is attempting to measure the amount of activity in each kidney as a function of time. These functions are approximated by time-activity curves obtained from ROIs over the kidneys. The resulting time-activity curves have components that are due to the detection of extrarenal (i.e., background) activity. In addition, there is attenuation of photons from the kidney due to the intervening tissue. Thus, in order to estimate the activity in each kidney, it is desirable to attempt to correct for background activity and attenuation.

Background and attenuation correction for renography is a somewhat controversial subject

that is an area of ongoing research. We limit ourselves here to describing some simple first-order corrections that illustrate the general ideas involved and that are adequate except in the case of extremely poor renal function. For more sophisticated approaches, we refer the reader to the literature.

Background correction is usually based on the time-activity curve obtained from an ROI adjacent to the kidneys. This ROI is termed the background region. Various background regions have been proposed: an area between the kidneys, an area around the kidneys, an area superior to the kidneys, and an area inferolateral to the kidney have been used [147–149].

A simple approach to *background correction* is as follows: Let $K(t)$ and $B(t)$ denote the kidney and background time-activity curves, respectively. Let A_K and A_B denote the area in pixels of the renal and background ROIs, respectively. The background-corrected kidney time-activity curve, $K_c(t)$, is computed using the formula

$$K_c(t) = K(t) - S(A_K / A_B) B(t),$$

where S is a scaling factor (usually equal to 1) [147].

More sophisticated techniques for background correction take into account such factors as kidney volume and differences in kinetics between the kidney and background curves [150, 151]. The use of such techniques reportedly results in more accurate quantification of renal function [151].

A simple approach to *attenuation correction* is based on the mean distance of the kidney from the surface of the body. This distance may be measured by the gamma camera using a lateral view or by ultrasonography. Alternatively, this distance may be estimated from the patient's height and weight using a nomogram [152]. Attenuation correction is done by multiplying the background-corrected renal time-activity curve by e^{ux}, where u is the linear attenuation coefficient of the radiotracer in soft tissues and x is the mean distance of the kidney from the surface of the body [149, 153]. A more sophisticated approach may be found in the paper by Takaki et al. [151].

Deconvolution Analysis

After background and attenuation correction, the renal time-activity curve approximates the amount of tracer in the kidney as a function of time. It is intuitively clear that this time-activity curve depends on how much radiotracer enters the kidney from the bloodstream as a function of time, which we refer to as the input function, as well as the handling of the radiotracer by the kidney. The input function and hence the observed renal time-activity curve are affected by factors that have no bearing on the function of a particular kidney, such as the function of the other kidney, loss of radiotracer from the intravascular space, and, occasionally, continued input of radiotracer from a partially extravasated injection [154]. The purpose of deconvolution analysis is to describe the handling of the tracer by the kidney in a way that is independent of the input function.

One way to describe the handling of radiotracer by the kidney is to construct a curve showing the fraction of radiotracer entering the kidney at time 0, and the fraction that remains in the kidney at time t. We call this curve the retention function. The retention function is of direct clinical significance. For example, prolonged retention of radiotracer suggests obstruction. It is intuitively clear that the observed renal curve is determined by the input function and the retention function. To make this statement mathematically precise, the kidney is modeled as a linear, time-invariant system whose input is the input function discussed above and whose unit impulse response is equal to the retention function. With this model, the observed renal curve is given by the mathematical operation of convolution of the input function and the retention function. Denoting the input, retention, and kidney functions by $I(t)$, $R(t)$, and $K(t)$, respectively, we can write it as

$$K(t) = I(t) * R(t),$$

where * denotes the mathematical operation of convolution. Given $I(t)$ and $K(t)$, one can solve this equation for $R(t)$. This is known as deconvolution. The concepts of linear, time-invariant

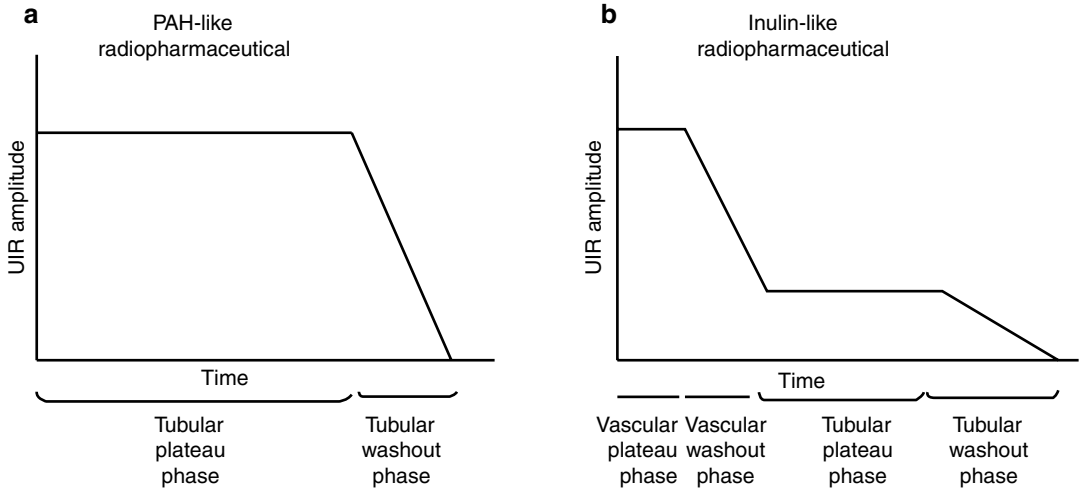

Fig. 12.46 (**a**) Deconvoluted renal time-activity histogram from a substance behaving like para-aminohippuric acid (*PAH*). (**b**) Deconvoluted renal time-activity curve from a substance behaving like inulin

system, unit impulse response, convolution, and so forth are discussed in more detail by Oppenheim et al. [155].

The input function is commonly assumed to be proportional to the plasma tracer concentration in the blood entering the kidney. This function is difficult to measure directly. In practice, the input function may be approximated as being proportional to a time-activity curve obtained from the abdominal aorta, heart, liver, or brain [154, 156]. There are two possible sources of error in this approximation: temporal differences in tracer concentration between the plasma in the pool being monitored and the renal artery and possible contamination of the observed blood-pool curve by detection of extravascular activity. However, this approximation of the input function by externally detected time-activity curves has been found to work well in practice [157].

Several investigators have reported using deconvolution to estimate the renal retention function [57, 147, 154, 158]. One difficulty with deconvolution is that small observation errors may lead to physiologically unrealistic negative values and high-frequency oscillations in the computed retention function [159]. To prevent this, we have found it useful to introduce constraints derived from physiologic considerations of the renal system into the deconvolution process. Specifically, the computed retention function is constrained to be nonnegative and nonincreasing. Retention functions computed using this technique have been shown to be relatively insensitive to random data errors [160].

Interpretation of the Renal Retention Function

The computed retention function is an estimate of the renal time-activity curve that would be obtained after an instantaneous intra-arterial injection of a radiotracer without recirculation. Consider such a curve obtained with a PAH-like substance that is handled primarily by tubular secretion (e.g., ^{123}I-OIH). All of the tracer arriving in the kidney subsequently enters the tubular space by either glomerular filtration or tubular secretion and leaves via the ureter. The corresponding retention function, shown in Fig. 12.46a, consists of a tubular plateau phase (from time 0 to the minimal tubular transit time) followed by a tubular washout phase. In contrast, consider such a curve obtained with a substance like inulin that is handled primarily by glomerular filtration (e.g., ^{99m}Tc-DTPA). A fraction of the tracer, equal to the filtration fraction, enters the tubular space by

glomerular filtration and leaves via the ureter. The remainder of tracer stays in the vascular space and leaves the kidney via the renal vein. The corresponding retention function, shown in Fig. 12.46b, consists of a vascular plateau phase (from time 0 until the minimal vascular transit time), a vascular washout phase (until the maximal vascular transit time), a tubular plateau phase (until the minimal tubular transit time), and a tubular washout phase. The amplitude of the tubular plateau divided by the amplitude of the vascular plateau is equal to the filtration fraction. The vascular phase occurs quite rapidly, however, and is difficult to delineate at the frame rates commonly used for dynamic renal imaging. It is sometimes useful for interpretation to eliminate the vascular phase of the retention function by setting the retention function values prior to a set time (chosen to be greater than the maximal vascular transit time and less than the minimal tubular transit time) equal to the retention function value at that time. The resulting curve is termed the tubular retention function.

Computed retention functions may be used to calculate indices of relative renal function (i.e., left versus right). Relative effective renal plasma flow (ERPF) may be estimated from the relative initial amplitudes of the retention functions obtained using a tracer that is handled like PAH [147, 158]. Relative GFR may be estimated from the relative initial amplitudes of the tubular retention functions obtained using a tracer that is handled like inulin [154]. Relative GFR calculated by this method has been shown to correlate well with individual kidney creatinine clearance [161]. Computed retention functions are also useful for quantifying transit times of radiotracer through the kidney. The mean tubular transit time (MTTT) (i.e., the mean time that filtered or secreted radiotracer remains in the kidney) has been shown to be of value for distinguishing obstructive from nonobstructive renal disease [156]. The MTTT may be computed using the formula

$$\mathrm{MTTT} = \int_0^\infty t\left(-dR\left(t\right)/\mathrm{dt}\right)\mathrm{dt},$$

where $R(t)$ is the tubular retention function [151].

Glomerular Filtration Rate

The GFR may be estimated following intravenous injection of a radiotracer that is handled like inulin (see Chap. 13). The substance most commonly used for this purpose is ^{99m}Tc-DTPA. There are two basic approaches to the estimation of GFR. The first approach is based on clearance of the radiotracer from the plasma, and the second approach is based on the rate of tracer uptake by the kidney. Both approaches are reasonable, and the choice between them is a matter of convenience.

With the plasma clearance method, it is assumed that the radiotracer leaves the body solely through the urine. Single-injection techniques have largely replaced the classic, but tedious, constant-infusion techniques and have been shown to correlate well with results obtained using the constant-infusion technique [162, 163]. The concentration of the tracer in the plasma as a function of time may be monitored by counting a series of blood samples. Alternatively, plasma concentration of the tracer may be recorded by an external detector over the heart or head. The resulting time-activity curve must be calibrated by one or more blood samples. External detection introduces a possible source of error because activity outside of the intravascular space may be detected [164]. But has the advantage of reducing the number of blood samples needed [165, 166].

Equations for calculating the clearance of a radiotracer after a single injection are derived from either a single- or multiple-compartment model [167, 168]. The parameters of the model are estimated by fitting a single or multiple exponential curve to the plasma concentration curve [162, 163, 166, 169, 170, 171].

The other approach to estimation of GFR, based on the uptake of the tracer by the kidney, assumes that the radiotracer remains in the kidney for at least some fixed period of time after it enters (typically 2–3 min) [172, 173].

One goal has been to eliminate the need for blood sampling. As with the plasma clearance approach, this is done, in essence, by using an empirically derived approximation for the effective volume of distribution of the radiotracer.

Gates reported using such a method to estimate GFR from the percentage of the ^{99m}Tc-DTPA dose taken up by the kidneys during the 2- to 3-min interval after injection [149]. More recently, Gordon et al. have reported using such a method in children [174].

The percent uptake of ^{99m}Tc-DTPA during the 1- to 2-min interval after injection can be used to estimate differential renal function. With this method, it is possible to monitor changes in renal function in patients undergoing surgical or medical treatment for a variety of renal diseases. It is also possible to estimate differential GFR from the relative percentage of uptake by the two kidneys [175].

Effective Renal Plasma Flow

The effective renal plasma flow (ERPF) may be estimated in the same manner as GFR if a radiotracer is used that is handled as PAH rather than as inulin. The most commonly used radiotracers for this purpose are ^{99m}Tc-MAG3 and ^{123}I-OIH [171]. In practice, ERPF measured with tracers such as these are always slightly lower than the actual renal plasma flow because no substance is completely extracted in a single pass [176]. The plasma clearance and renal uptake approaches have both been used. The techniques used are essentially the same as those used for estimating GFR from inulin-like radiopharmaceuticals.

As with estimation of GFR, the concentration of the tracer in plasma may be followed by either multiple blood samples or external detection. The two methods have been found to produce similar results. Blaufox et al. found a good correlation in the measurement of ERPF using ^{131}I-OIH with serial blood sampling and external detection using a scintillation probe over the patient's head [167]. Similarly, Ram et al. and Razzak et al. found good agreement in the values of ERPF calculated by serial blood sampling and external detection over the precordium [177, 178]. Ram et al. reported a strong correlation between ERPF estimates obtained by single-exponential extrapolation of ^{125}I-OIH time-activity curves obtained from over the precordium and PAH clearance. Mackay et al. reported the estimation of ERPF from a ^{123}I-OIH time-activity curve obtained over the abdomen and a single blood sample using single-exponential extrapolation [179]. The ERPF estimates were found to correlate closely with PAH clearances but tended to be slightly lower. The average value was 89 % of the PAH clearance values. Heidenreich et al. reported their clinical experience in the estimation of ERPF from the clearance of ^{123}I-OIH in 153 children [180].

As in the case of estimating GFR, there has been much interest in procedures for estimating ERPF that require no external counting and only a single blood sample. Again, these procedures work by using an empirically derived approximation for the effective volume of distribution of the radiotracer. Such simplified techniques have been shown to produce reasonable estimates of ERPF in children [30].

The renal uptake approach to ERPF estimation has also been used [152]. Thompson et al. reported the renal uptake of ^{131}I-OIH in the 1- to 2-min interval after injection correlated with PAH clearances [181].

Relative ERPF may also be estimated from the relative percentage of uptake of the two kidneys [153, 180, 182]. Relative uptake of ^{123}I-OIH in the 0.5- to 2.5-min interval following injection has been shown to correlate with separate kidney PAH clearance values obtained by ureteral catheterization [121].

References

1. Cao X, Tetrault T, Fahey F, Treves T. Automated motion correction based on target tracking for dynamic nuclear medicine studies. Proc SPIE. 2008;6914(1):69142B.
2. Moretti M, Magnani C, Calzolari E, Roncarati E. Genitourinary tract anomalies: neonatal medical problems. Fetal Ther. 1986;1(2–3):114–5.
3. Seikaly M, Ho PL, Emmett L, Tejani A. The 12th Annual Report of the North American Pediatric Renal Transplant Cooperative Study: renal transplantation from 1987 through 1998. Pediatr Transplant. 2001;5(3):215–31.
4. National Institute of Diabetes and Digestive and Kidney Diseases (U.S.). Division of Kidney Urologic and Hematologic Diseases: United States renal data system …1993 annual data report. Bethesda, MD:

National Institutes of Health, National Institute of Diabetes and Digestive and Kidney Diseases, Division of Kidney, Urologic, and Hematologic Diseases; Urban Institute. Renal Research Program, University of Michigan, USRDS Coordinating Center; 1993. p. v.
5. Koenigsberg M, Blaufox MD, Freeman LM. Traumatic injuries of the renal vasculature and parenchyma. In: Freeman LM, Blaufox MD, editors. Radionuclide studies of the genitourinary system. New York: Grune & Stratton; 1975. ix, 220 p.
6. Burko H, Rhamy RK. Lower urinary tract problems related to infection: diagnosis and treatment. Pediatr Clin North Am. 1970;17(2):233–53.
7. Bois E, Feingold J, Benmaiz H, Briard ML. Congenital urinary tract malformations: epidemiologic and genetic aspects. Clin Genet. 1975;8(1):37–47.
8. Sheih CP, Liu MB, Hung CS, Yang KH, Chen WY, Lin CY. Renal abnormalities in schoolchildren. Pediatrics. 1989;84(6):1086–90.
9. Barakat AJ, Drougas JG. Occurrence of congenital abnormalities of kidney and urinary tract in 13,775 autopsies. Urology. 1991;38(4):347–50.
10. Taylor Jr A, Eshima D, Fritzberg AR, Christian PE, Kasina S. Comparison of iodine-131 OIH and technetium-99m MAG3 renal imaging in volunteers. J Nucl Med. 1986;27(6):795–803.
11. Bubeck B, Brandau W, Steinbacher M, et al. Technetium-99m labeled renal function and imaging agents: II. Clinical evaluation of ^{99m}Tc MAG3 (99mTc mercaptoacetylglycylglycylglycine). Int J Rad Appl Instrum B. 1988;15(1):109–18.
12. Jafri RA, Britton KE, Nimmon CC, et al. Technetium-99m MAG3, a comparison with iodine-123 and iodine-131 orthoiodohippurate, in patients with renal disorders. J Nucl Med. 1988;29(2):147–58.
13. Russell CD, Thorstad B, Yester MV, Stutzman M, Baker T, Dubovsky EV. Comparison of technetium-99m MAG3 with iodine-131 hippuran by a simultaneous dual channel technique. J Nucl Med. 1988;29(7):1189–93.
14. Russell CD, Thorstad BL, Yester MV, Stutzman M, Dubovsky EV. Quantitation of renal function with technetium-99m MAG3. J Nucl Med. 1988; 29(12):1931–3.
15. Taylor Jr A, Eshima D, Alazraki N. ^{99m}Tc-MAG3, a new renal imaging agent: preliminary results in patients. Eur J Nucl Med. 1987;12(10):510–4.
16. Gelfand MJ, Parisi MT, Treves ST. Pediatric radiopharmaceutical administered doses: 2010 North American consensus guidelines. J Nucl Med. 2011; 52(2):318–22.
17. Hsiao EM, Cao X, Zurakowski D, et al. Reduction in radiation dose in mercaptoacetyltriglycerine renography with enhanced planar processing. Radiology. 2011;261(3):907–15.
18. Atkins HL, Cardinale KG, Eckelman WC, Hauser W, Klopper JF, Richards P. Evaluation of 99mTc-DTPA prepared by three different methods. Radiology. 1971;98(3):674–7.
19. Cohen ML, Smith Jr FG, Mindell RS, Vernier RL. A simple, reliable method of measuring glomerular filtration rate using single, low dose sodium iothalamate I-131. Pediatrics. 1969;43(3):407–15.
20. Elwood CM, Sigman EM. The measurement of glomerular filtration rate and effective renal plasma flow in man by iothalamate 125-I and iodopyracet 131-I. Circulation. 1967;36(3):441–8.
21. Elwood CM, Sigman EM, Treger C. The measurement of glomerular filtration rate with ^{125}I-sodium iothalamate (Conray). Br J Radiol. 1967;40(476):581–3.
22. Gagnon JA, Schrier RW, Weis TP, Kokotis W, Mailloux LU. Clearance of iothalamate-125 I as a measure of glomerular filtration rate in the dog. J Appl Physiol. 1971;30(5):774–8.
23. Hauser W, Atkins HL, Nelson KG, Richards P. Technetium-99m DTPA: a new radiopharmaceutical for brain and kidney scanning. Radiology. 1970; 94(3):679–84.
24. Houwen B, Donker A, Woldring MG. Simultaneous determination of glomerular filtration rate with ^{125}I-iothalamate and effective renal plasma flow with ^{131}I-hippuran. Paper presented at: Dynamic studies with radioisotopes in medicine. Proceedings of the symposium … organized by the International Atomic Energy Agency, and held in Rotterdam, Vienna, 31 Aug–4 Sept 1970–1971.
25. Klopper JF, Hauser W, Atkins HL, Eckelman WC, Richards P. Evaluation of 99m Tc-DTPA for the measurement of glomerular filtration rate. J Nucl Med. 1972;13(1):107–10.
26. Kountz SL, Yeh SH, Wood J, Cohn R, Kriss JP. Technetium-99m(V)-citrate complex for estimation of glomerular filtration rate. Nature. 1967;215(108): 1397–9.
27. Maher FT, Nolan NG, Elveback LR. Comparison of simultaneous clearances of 125-I-labeled sodium iothalamate (Glofil) and of inulin. Mayo Clin Proc. 1971;46(10):690–1.
28. Oester A, Wolf H, Madsen PO. Double isotope technique in renal function testing in dogs. Invest Urol. 1969;6(4):387–92.
29. Sigman EM, Elwood C, Reagan ME, Morris AM, Catanzaro A. The renal clearance of I-131 labelled sodium iothalamate in man. Invest Urol. 1965;15: 432–8.
30. Russell CD, Bischoff PG, Rowell KL, et al. Quality control of Tc-99m DTPA for measurement of glomerular filtration: concise communication. J Nucl Med. 1983;24(8):722–7.
31. McAfee JG, Gagne G, Atkins HL, et al. Biological distribution and excretion of DTPA labeled with Tc-99m and In-111. J Nucl Med. 1979;20(12):1273–8.
32. Arnold RW, Subramanian G, McAfee JG, Blair RJ, Thomas FD. Comparison of 99mTc complexes for renal imaging. J Nucl Med. 1975;16(5):357–67.
33. Lee HB, Blaufox MD. Mechanism of renal concentration of technetium-99m glucoheptonate. J Nucl Med. 1985;26(11):1308–13.
34. Tubis M, Posnick E, Nordyke RA. Preparation and use of I 131 labeled sodium iodohippurate in kidney function tests. Proc Soc Exp Biol Med. 1960;103:497–8.

35. Chervu LR, Freeman LM, Blaufox MD. Radiopharmaceuticals for renal studies. Semin Nucl Med. 1974;4(1):3–22.
36. Mailloux LU, Gagnon JA. Measurement of effective renal plasma flow. In: Blaufox MD, editor. *Progress in Nuclear Medicine*. Baltimore: University Park Press; 1972. xiv, 315 p.
37. Howman-Giles R, Uren R, Roy LP, Filmer RB. Volume expansion diuretic renal scan in urinary tract obstruction. J Nucl Med. 1987;28(5):824–8.
38. Nauta J, Pot DJ, Kooij PP, Nijman JM, Wolff ED. Forced hydration prior to renography in children with hydronephrosis. An evaluation. Br J Urol. 1991;68(1): 93–7.
39. Sukhai RN, Kooy PP, Wolff ED, Scholtmeijer RJ. Predictive value of ^{99m}Tc-DTPA renography studies under conditions of maximal diuresis for the functional outcome of reconstructive surgery in children with obstructive uropathy. Br J Urol. 1986;58(6):596–600.
40. Treves ST, Packard AB, Fung LC. Assessment of rapid changes in renal blood flow with (^{191m})Ir, an ultra-short-lived radionuclide. J Nucl Med. 2004; 45(3):508–11.
41. Treves ST, Fung L, Packard AB. Rapid renal single-photon emission tomography by continuous infusion of iridium-191m. Eur J Nucl Med. 1999;26(5): 489–93.
42. Shore RM, Uehling DT, Bruskewitz R, Polcyn RE. Evaluation of obstructive uropathy with diuretic renography. Am J Dis Child. 1983;137(3):236–40.
43. Koff SA, Thrall JH, Keyes Jr JW. Assessment of hydroureteronephrosis in children using diuretic radionuclide urography. J Urol. 1980;123(4):531–4.
44. Mesrobian HG, Perry JR. Radionuclide diuresis pyelography. J Urol. 1991;146(2 Pt 2):601–4.
45. Thrall JH, Koff SA, Keyes Jr JW. Diuretic radionuclide renography and scintigraphy in the differential diagnosis of hydroureteronephrosis. Semin Nucl Med. 1981;11(2):89–104.
46. Meller ST, Eckstein HB. Renal scintigraphy: quantitative assessment of upper urinary tract dilatation in children. J Pediatr Surg. 1981;16(2):126–33.
47. Enlander D, Weber PM, dos Remedios LV. Renal cortical imaging in 35 patients: superior quality with 99mTc-DMSA. J Nucl Med. 1974;15(9):743–9.
48. Kawamura J, Hosokawa S, Yoshida O. Renal function studies using ^{99m}Tc-dimercaptosuccinic acid. Clin Nucl Med. 1979;4(1):39–46.
49. Willis KW, Martinez DA, Hedley-Whyte ET, Davis MA, Judy PF, Treves S. Renal localization of ^{99m}Tc-stannous glucophetonate and ^{99m}Tc-stannous dimercaptosuccinate in the rat by frozen section autoradiography. The efficiency and resolution of technetium-99m. Radiat Res. 1977;69(3):475–88.
50. Daly MJ, Jones WA, Rudd TG, Tremann JA. Differential ^{99m}Tc dimercaptosuccinic acid (DMSA) renal localization: correlation with renal function. J Nucl Med. 1977;18:594–5.
51. Daly MJ, Jones W, Rudd TG, Tremann J. Differential renal function using technetium-99m dimercaptosuccinic acid (DMSA): in vitro correlation. J Nucl Med. 1979;20(1):63–6.
52. Taylor Jr A. Quantitation of renal function with static imaging agents. Semin Nucl Med. 1982;12(4):330–44.
53. Gittes RF, Rist M, Treves S, Biewiner A. Autoregulation in rats with transplanted supernumerary kidneys. Nature. 1980;284(5757):618–20.
54. Sheehy N, Tetrault TA, Zurakowski D, Vija AH, Fahey FH, Treves ST. Pediatric 99mTc-DMSA SPECT performed by using iterative reconstruction with isotropic resolution recovery: improved image quality and reduced radiopharmaceutical activity. Radiology. 2009;251(2):511–6.
55. Cao X, Zurakowski D, Diamond DA, Treves ST. Automatic measurement of renal volume in children using ^{99m}Tc dimercaptosuccinic acid SPECT: normal ranges with body weight. Clin Nucl Med. 2012;37(4):356–61.
56. Treves ST, Baker A, Fahey FH, et al. Nuclear medicine in the first year of life. J Nucl Med. 2011; 52(6):905–25.
57. Vanpee M, Blennow M, Linne T, Herin P, Aperia A. Renal function in very low birth weight infants: normal maturity reached during early childhood. J Pediatr. 1992;121(5 Pt 1):784–8.
58. Dunbar JS, Nogrady B. Excretory urography in the first year of life. Radiol Clin North Am. 1972; 10(2):367–91.
59. Martin DJ, Gilday DL, Reilly BJ. Evaluation of the urinary tract in the neonatal period. Radiol Clin North Am. 1975;13(2):359–68.
60. Slutsky LJ, Golimbu M, Braunstein P, Al-Askari S, Genieser N, Golimbu C. Urographic imaging in neonatal period: radionuclide scan and x-ray. Urology. 1977;10(2):169–72.
61. Sherman RA, Blaufox MD. Obstructive uropathy in patients with nonvisualization on renal scan. Nephron. 1980;25(2):82–6.
62. Chung YK, Chang PY, Lin CJ, Wang NL, Sheu JC, Shih BF. Conservative treatment of neonatal hydronephrosis. J Formos Med Assoc. 1992;91(1):75–80.
63. Gordon I, Dhillon HK, Peters AM. Antenatal diagnosis of renal pelvic dilatation–the natural history of conservative management. Pediatr Radiol. 1991;21(4): 272–3.
64. Homsy YL, Saad F, Laberge I, Williot P, Pison C. Transitional hydronephrosis of the newborn and infant. J Urol. 1990;144(2 Pt 2):579–83; discussion 593–4.
65. Ransley PG, Dhillon HK, Gordon I, Duffy PG, Dillon MJ, Barratt TM. The postnatal management of hydronephrosis diagnosed by prenatal ultrasound. J Urol. 1990;144(2 Pt 2):584–7; discussion 593–84.
66. Samuelson U, Granerus G, Bjures J, Hagberg S, Hjalmas K. Renal function in idiopathic hydronephrosis in children. Follow-up after conservative and surgical treatment. Scand J Urol Nephrol. 1984;18(2): 135–41.
67. Djurhuus JC, Dorph S, Christiansen L, Ladefoged J, Nerstrom B. Predictive value of renography and i.v.

urography for the outcome of reconstructive surgery in patients with hydronephrosis. Acta Chir Scand Suppl. 1976;472:37–41.
68. McAfee JG, Singh A, O'Callaghan JP. Nuclear imaging supplementary to urography in obstructive uropathy. Radiology. 1980;137(2):487–96.
69. Kalika V, Bard RH, Iloreta A, Freeman LM, Heller S, Blaufox MD. Prediction of renal functional recovery after relief of upper urinary tract obstruction. J Urol. 1981;126(3):301–5.
70. Jamar F, Piret L, Wese FX, Beckers C. Influence of ureteral status on kidney washout during technetium-99m-DTPA diuresis renography in children. J Nucl Med. 1992;33(1):73–8.
71. Busch R, Huland H. Correlation of symptoms and results of direct bacterial localization in patients with urinary tract infections. J Urol. 1984;132(2):282–5.
72. Majd M, Rushton HG, Jantausch B, Wiedermann BL. Relationship among vesicoureteral reflux, P-fimbriated Escherichia coli, and acute pyelonephritis in children with febrile urinary tract infection. J Pediatr. 1991;119(4):578–85.
73. Jacobson SH, Eklof O, Eriksson CG, Lins LE, Tidgren B, Winberg J. Development of hypertension and uraemia after pyelonephritis in childhood: 27 year follow up. BMJ. 1989;299(6701):703–6.
74. Glauser MP, Lyons JM, Braude AI. Prevention of chronic experimental pyelonephritis by suppression of acute suppuration. J Clin Invest. 1978;61(2):403–7.
75. Miller T, Phillips S. Pyelonephritis: the relationship between infection, renal scarring, and antimicrobial therapy. Kidney Int. 1981;19(5):654–62.
76. Slotki IN, Asscher AW. Prevention of scarring in experimental pyelonephritis in the rat by early antibiotic therapy. Nephron. 1982;30(3):262–8.
77. Bjorgvinsson E, Majd M, Eggli KD. Diagnosis of acute pyelonephritis in children: comparison of sonography and ^{99m}Tc-DMSA scintigraphy. AJR Am J Roentgenol. 1991;157(3):539–43.
78. Farnsworth RH, Rossleigh MA, Leighton DM, Bass SJ, Rosenberg AR. The detection of reflux nephropathy in infants by ^{99m}technetium dimercaptosuccinic acid studies. J Urol. 1991;145(3):542–6.
79. Jantausch BA, Wiedermann BL, Hull SI, et al. Escherichia coli virulence factors and ^{99m}Tc-dimercaptosuccinic acid renal scan in children with febrile urinary tract infection. Pediatr Infect Dis J. 1992;11(5):343–9.
80. Kass EJ, Fink-Bennett D, Cacciarelli AA, Balon H, Pavlock S. The sensitivity of renal scintigraphy and sonography in detecting nonobstructive acute pyelonephritis. J Urol. 1992;148(2 Pt 2):606–8.
81. Majd M, Rushton HG. Renal cortical scintigraphy in the diagnosis of acute pyelonephritis. Semin Nucl Med. 1992;22(2):98–111.
82. Rushton HG, Majd M, Jantausch B, Wiedermann BL, Belman AB. Renal scarring following reflux and nonreflux pyelonephritis in children: evaluation with ^{99m}technetium-dimercaptosuccinic acid scintigraphy. J Urol. 1992;147(5):1327–32.
83. Verber IG, Meller ST. Serial ^{99m}Tc dimercaptosuccinic acid (DMSA) scans after urinary infections presenting before the age of 5 years. Arch Dis Child. 1989;64(11):1533–7.
84. Goldraich NP, Ramos OL, Goldraich IH. Urography versus DMSA scan in children with vesicoureteric reflux. Pediatr Nephrol. 1989;3(1):1–5.
85. Itoh K, Asano Y, Tsukamoto E, et al. Single photon emission computed tomography with Tc-99m-dimercaptosuccinic acid in patients with upper urinary tract infection and/or vesicoureteral reflux. Ann Nucl Med. 1991;5(1):29–34.
86. Verboven M, Ingels M, Delree M, Piepsz A. ^{99m}Tc-DMSA scintigraphy in acute urinary tract infection in children. Pediatr Radiol. 1990;20(7):540–2.
87. Merrick MV, Uttley WS, Wild SR. The detection of pyelonephritic scarring in children by radioisotope imaging. Br J Radiol. 1980;53(630):544–56.
88. Handmaker H. Nuclear renal imaging in acute pyelonephritis. Semin Nucl Med. 1982;12(3):246–53.
89. Jakobsson B, Nolstedt L, Svensson L, Soderlundh S, Berg U. ^{99m}Technetium-dimercaptosuccinic acid scan in the diagnosis of acute pyelonephritis in children: relation to clinical and radiological findings. Pediatr Nephrol. 1992;6(4):328–34.
90. Tappin DM, Murphy AV, Mocan H, et al. A prospective study of children with first acute symptomatic E. coli urinary tract infection. Early ^{99m}technetium dimercaptosuccinic acid scan appearances. Acta Paediatr Scand. 1989;78(6):923–9.
91. Applegate KE, Connolly LP, Davis RT, Zurakowski D, Treves ST. A prospective comparison of high-resolution planar, pinhole, and triple-detector SPECT for the detection of renal cortical defects. Clin Nucl Med. 1997;22(10):673–8.
92. Joseph DB, Young DW, Jordon SP. Renal cortical scintigraphy and single proton emission computerized tomography (SPECT) in the assessment of renal defects in children. J Urol. 1990;144(2 Pt 2):595–7; discussion 606.
93. Roberts JA, Roth Jr JK, Domingue G, Lewis RW, Kaack B, Baskin G. Immunology of pyelonephritis in the primate model. V. Effect of superoxide dismutase. J Urol. 1982;128(6):1394–400.
94. Kaack MB, Dowling KJ, Patterson GM, Roberts JA. Immunology of pyelonephritis. VIII. E. coli causes granulocytic aggregation and renal ischemia. J Urol. 1986;136(5):1117–22.
95. Androulakakis PA, Ransley PG, Risdon RA, Sorger K, Hohenfellner R. Microvascular changes in the early stage of reflux pyelonephritis. An experimental study in the pig kidney. Eur Urol. 1987;13(4):219–23.
96. Elink M. Emergency uroradiology for the nontraumatized patient. Radiol Clin North Am. 1978;16(1):135–46.
97. Handmaker H, Young BW, Lowenstein JM. Clinical experience with ^{99m}Tc-DMSA (dimercaptosuccinic acid), a new renal-imaging agent. J Nucl Med. 1975;16(1):28–32.

98. Silver TM, Kass EJ, Thornbury JR, Konnak JW, Wolfman MG. The radiological spectrum of acute pyelonephritis in adults and adolescents. Radiology. 1976;118(1):65–71.
99. Kahn PC. Renal imaging with radionuclides, ultrasound, and computed tomography. Semin Nucl Med. 1979;9(1):43–57.
100. June CH, Browning MD, Smith LP, et al. Ultrasonography and computed tomography in severe urinary tract infection. Arch Intern Med. 1985;145(5):841–5.
101. Montgomery P, Kuhn JP, Afshani E. CT evaluation of severe renal inflammatory disease in children. Pediatr Radiol. 1987;17(3):216–22.
102. Raynaud C, Tran-Dinh S, Bourguignon M, et al. Acute pyelonephritis in children. Preliminary results obtained with NMR imaging. Contrib Nephrol. 1987;56:129–34.
103. Arneil GC, MacDonald AM, Sweet EM. Renal venous thrombosis. Clin Nephrol. 1973;1(3):119–31.
104. Avery ME, Oppenheimer EH, Gordon HH. Renal-vein thrombosis in newborn infants of diabetic mothers; report of 2 cases. N Engl J Med. 1957;256(24):1134–8.
105. Kaufmann HJ. Renal vein thrombosis. 1. Age incidence in infancy and childhood. 2. Sex incidence. 3. Incidence of unilateral and bilateral involvement. AMA J Dis Child. 1958;95(4):377–84.
106. Rasoulpour M, McLean RH. Renal venous thrombosis in neonates. Initial and follow-up abnormalities. Am J Dis Child. 1980;134(3):276–9.
107. Stark H. Renal vein thrombosis in infancy. Recovery without nephrectomy. Am J Dis Child. 1964;108:430–5.
108. Takeuchi A, Benirschke K. Renal venous thrombosis of the newborn and its relation to maternal diabetes. Report of 16 cases. Biol Neonat. 1961;3:237–56.
109. Verhagen AD, Hamilton JP, Genel M. Renal vein thrombosis in infants. Arch Dis Child. 1965;40:214–7.
110. Duncan RE, Evans AT, Martin LW. Natural history and treatment of renal vein thrombosis in children. J Pediatr Surg. 1977;12(5):639–45.
111. Quigley JM, Druy EM, Rich JI. Acute renal vein thrombosis with a diagnostic renal scintigram. AJR Am J Roentgenol. 1981;137(5):1066–8.
112. Blaufox MD. Systemic arterial hypertension in pediatric practice. Pediatr Clin North Am. 1971;18(2):577–93.
113. Ingelfinger JR. Pediatric hypertension. Philadelphia: Saunders; 1982.
114. Londe S. Causes of hypertension in the young. Pediatr Clin North Am. 1978;25(1):55–65.
115. Olson DL, Lieberman E. Renal hypertension in children. Pediatr Clin North Am. 1976;23(4):795–805.
116. Rosen PR, Treves S. The efficacy of ^{99m}Tc screening of pediatric patients for renal etiologies in hypertension. J Nucl Med. 1983;24(5):22.
117. Geyskes GG, Oei HY, Puylaert CB, Dorhout Mees EJ. Renography with captopril. Changes in a patient with hypertension and unilateral renal artery stenosis. Arch Intern Med. 1986;146(9):1705–8.
118. Majd M, Potter BN, Guzzeta PC, Ruley EJ. Effect of captopril on efficacy of renal scintigraphy in detection of renal artery stenosis [abstract]. J Nucl Med. 1983;24:23.
119. Sfakianakis GN, Sfakianaki E, Bourgoignie J. Lasix captopril renography in the diagnosis of renovascular hypertension. Contrib Nephrol. 1990;79:219–27.
120. Siegel MJ, St Amour TE, Siegel BA. Imaging techniques in the evaluation of pediatric hypertension. Pediatr Nephrol. 1987;1(1):76–88.
121. Wenting GJ, Tan-Tjiong HL, Derkx FH, de Bruyn JH, Man in't Veld AJ, Schalekamp MA. Splint renal function after captopril in unilateral renal artery stenosis. Br Med J (Clin Res Ed). 1984;288(6421):886–90.
122. Vivan G, Stringer D, DeBruyn R, et al. ^{99m}Tc DMSA in renovascular hypertension in children. Paper presented at: Nuclear medicine and biology advances: proceedings of the Third World Congress of Nuclear Medicine and Biology, August 29 to September 2, 1982, Paris, France. Oxford [Oxfordshire]/New York, 1983.
123. Minty I, Lythgoe MF, Gordon I. Hypertension in paediatrics: can pre- and post-captopril technetium-99m dimercaptosuccinic acid renal scans exclude renovascular disease? Eur J Nucl Med. 1993;20(8):699–702.
124. Dondi M. Captopril renal scintigraphy with ^{99m}Tc-mercaptoacetyltriglycine (^{99m}Tc-MAG3) for detecting renal artery stenosis. Am J Hypertens. 1991;4(12 Pt 2):737S–40.
125. Dondi M, Fanti S, De Fabritiis A, et al. Prognostic value of captopril renal scintigraphy in renovascular hypertension. J Nucl Med. 1992;33(11):2040–4.
126. Oei HY. Captopril renography. Early observations and diagnostic criteria. Am J Hypertens. 1991;4(12 Pt 2):678S–84.
127. Setaro JF, Chen CC, Hoffer PB, Black HR. Captopril renography in the diagnosis of renal artery stenosis and the prediction of improvement with revascularization. The Yale Vascular Center experience. Am J Hypertens. 1991;4(12 Pt 2):698S–705.
128. Hildebrandt O. Anatomie der Nierengeschwulste. Arch Klin Chir. 1894;48:343.
129. Bernstein J. The morphogenesis of renal parenchymal maldevelopment (renal dysplasia). Pediatr Clin North Am. 1971;18(2):395–407.
130. Zerres K, Volpel MC, Weiss H. Cystic kidneys. Genetics, pathologic anatomy, clinical picture, and prenatal diagnosis. Hum Genet. 1984;68(2):104–35.
131. Berdon WE, Baker DH, Wigger HJ, Blanc WA. The radiologic and pathologic spectrum of the prune belly syndrome. The importance of urethral obstruction in prognosis. Radiol Clin North Am. 1977;15(1):83–92.
132. Guthrie L. Case of congenital deficiency of the abdominal muscles with dilatation and hypertrophy of the bladder ureters. Trans Pathol Soc Lond. 1918;47:139–45.
133. Parker RW. Case of an infant in whom some of the abdominal muscles were absent. Trans Clin Soc Lond. 1895;28:201–3.

134. Williams DI, Burkholder GV. The prune belly syndrome. J Urol. 1967;98(2):244–51.
135. Leonard JC, Allen EW, Goin J, Smith CW. Renal cortical imaging and the detection of renal mass lesions. J Nucl Med. 1979;20(10):1018–22.
136. Older RA, Korobkin M, Workman J, et al. Accuracy of radionuclide imaging in distinguishing renal masses from normal variants. Radiology. 1980;136(2):443–8.
137. Parker JA, Lebowitz R, Mascatello V, Treves S. Magnification renal scintigraphy in the differential diagnosis of septa of Bertin. Pediatr Radiol. 1976;4(3):157–60.
138. Awad W, Bennett LR, Martin DC. Detection of renal homograft rejection reaction with a single dose of radiohippuran. J Urol. 1968;100(3):233–7.
139. Awad W, Boake RC, Bennett LR, Martin DC. Double isotope scan in kidney transplantation. Am Surg. 1968;34(11):768–74.
140. Figueroa JE, Maxfield WS, Batson HM, Birchall R. Radioisotope renal function studies in human renal allografts: value in the differential diagnosis of oliguria in the presence of obstructive disease with and without urinary extravasation. J Urol. 1968;100(2): 104–8.
141. Lubin E, Lewitus Z, Rosenfield J, Levi N. Kidney scanning with hippuran, a necessary complement for correct interpretation of renography in the transplanted kidney. Paper presented at: Medical radioisotope scintigraphy. Proceedings of a symposium … held by the International Atomic Energy Agency in Salzburg, Vienna, 6–15 Aug 1968–1969.
142. Magnusson G, Collste L, Franksson C, Lundgren G. Radiorenography in clinical transplantation. Scand J Urol Nephrol. 1967;1:132–51.
143. Treves ST, Lebowitz R, Kuruc A, Heyman S, Rose P. Kidneys. In: Treves S, editor. Pediatric nuclear medicine. New York: Springer; 1985. p. 63–103.
144. Zum Winkel K, Harbst H, Schenck P, et al. Sequential scintigraphy in renal transplantation. Paper presented at: Medical radioisotope scintigraphy. Proceedings of a symposium … held by the International Atomic Energy Agency in Salzburg, Vienna, 6–15 Aug 1968–1969.
145. Harmon WE, Stablein D, Alexander SR, Tejani A. Graft thrombosis in pediatric renal transplant recipients. A report of the North American Pediatric Renal Transplant Cooperative Study. Transplantation. 1991;51(2):406–12.
146. Spigos DG, Tan W, Pavel DG, Mozes M, Jonasson O, Capek V. Diagnosis of urine extravasation after renal transplantation. AJR Am J Roentgenol. 1977; 129(3):409–13.
147. Kenny RW, Ackery DM, Fleming JS, Goddard BA, Grant RW. Deconvolution analysis of the scintillation camera renogram. Br J Radiol. 1975;48(570): 481–6.
148. Short MD, Glass HI, Chisholm GD, Vernon P, Silvester DJ. Gamma-camera renography using ^{123}I-hippuran. Br J Radiol. 1973;46(544):289–94.
149. Gates GF. Glomerular filtration rate: estimation from fractional renal accumulation of ^{99m}Tc-DTPA (stannous). AJR Am J Roentgenol. 1982;138(3):565–70.
150. Decostre PL, Salmon Y. Temporal behavior of peripheral organ distribution volume in mammillary systems. II. Application to background correction in separate glomerular filtration rate estimation in man. J Nucl Med. 1990;31(10):1710–6.
151. Takaki Y, Kojima A, Tsuji A, Nakashima R, Tomiguchi S, Takahashi M. Quantification of renal uptake of technetium-99m-DTPA using planar scintigraphy: a technique that considers organ volume. J Nucl Med. 1993;34(7):1184–9.
152. Schlegel JU, Hamway SA. Individual renal plasma flow determination in 2 minutes. J Urol. 1976; 116(3):282–5.
153. Moser E, Jocham D, Beer M, Bull U. Effects of obstruction on single-kidney function: clinical and experimental results with ^{131}I-hippurate and ^{99m}Tc-DMSA. Nuklearmedizin. 1980;19(6):257–62.
154. Diffey BL, Hall FM, Corfield JR. The ^{99m}Tc-DTPA dynamic renal scan with deconvolution analysis. J Nucl Med. 1976;17(5):352–5.
155. Oppenheim AV, Willsky AS, Young IT. Signals and systems. Englewood Cliffs, N.J.: Prentice-Hall; 1983.
156. Piepsz A, Ham HR, Erbsmann F, et al. A co-operative study on the clinical value of dynamic renal scanning with deconvolution analysis. Br J Radiol. 1982;55(654):419–33.
157. Erbsmann F, Strugven J, Ham H, Piepsz A. Analysis of errors and systemic biases in the calculation of the renal retention function. Paper presented at: Information Processing in Medical Imaging (Proceedings of the Vth International Conference), Nashville, 1978.
158. Fleming JS, Goddard BA. A technique for the deconvolution of the renogram. Phys Med Biol. 1974;19(4): 546–9.
159. Gamel J, Rousseau WF, Katholi CR, Mesel E. Pitfalls in digital computation of the impulse response of vascular beds from indicator-dilution curves. Circ Res. 1973;32(4):516–23.
160. Kuruc A, Caldicott WJ, Treves S. An improved deconvolution technique for the calculation of renal retention functions. Comput Biomed Res. 1982;15(1):46–56.
161. Kainer G, McIlveen B, Hoschl R, Rosenberg AR. Assessment of individual renal function in children using ^{99m}Tc-DTPA. Arch Dis Child. 1979;54(12): 931–6.
162. Huttunen K, Huttunen NP, Koivula A, Ahonen A, Puukka R. ^{99m}Tc-DTPA–a useful clinical tool for the measurement of glomerular filtration rate. Scand J Urol Nephrol. 1982;16(3):237–41.
163. Powers TA, Stone WJ, Grove RB, et al. Radionuclide measurement of differential glomerular filtration rate. Invest Radiol. 1981;16(1):59–64.
164. Kuruc A, Treves ST, Rosen PR, Greenberg D. Estimating the plasma time-activity curve during

radionuclide renography. J Nucl Med. 1987;28(8): 1338–40.
165. Owen JE, Walker RG, Willems D, Guignard PA, d'Apice AJ. Cadmium telluride detectors in the external measurement of glomerular filtration rate using ^{99m}Tc-DTPA (Sn): comparison with ^{51}Cr-EDTA and ^{99m}Tc-DTPA (Sn) plasma sample methods. Clin Nephrol. 1982;18(4):200–3.
166. Rossing N, Bojsen J, Frederiksen PL. The glomerular filtration rate determined with ^{99m}Tc-DTPA and a portable cadmium telluride detector. Scand J Clin Lab Invest. 1978;38(1):23–8.
167. Blaufox MD, Potchen EJ, Merrill JP. Measurement of effective renal plasma flow in man by external counting methods. J Nucl Med. 1967;8(2):77–85.
168. Sapirstein LA, Vidt DG, Mandel MJ, Hanusek G. Volumes of distribution and clearances of intravenously injected creatinine in the dog. Am J Physiol. 1955;181(2):330–6.
169. Rootwelt K, Falch D, Sjokvist R. Determination of glomerular filtration rate (GFR) by analysis of capillary blood after single shot injection of ^{99m}Tc-DTPA. A comparison with simultaneous 125I-iothalamate GFR estimation showing equal GFR but difference in distribution volume. Eur J Nucl Med. 1980;5(2):97–102.
170. Hall JE, Guyton AC, Farr BM. A single-injection method for measuring glomerular filtration rate. Am J Physiol. 1977;232(1):F72–6.
171. Ham HR, Piepsz A. Estimation of glomerular filtration rate in infants and in children using a single-plasma sample method. J Nucl Med. 1991;32(6):1294–7.
172. Piepsz A, Dobbeleir A, Erbsmann F. Measurement of separate kidney clearance by means of ^{99m}Tc-DTPA complex and a scintillation camera. Eur J Nucl Med. 1977;2(3):173–7.
173. Piepsz A, Denis R, Ham HR, Dobbeleir A, Schulman C, Erbsmann F. A simple method for measuring separate glomerular filtration rate using a single injection of ^{99m}Tc-DTPA and the scintillation camera. J Pediatr. 1978;93(5):769–74.
174. Gordon I, Anderson PJ, Orton M, Evans K. Estimation of technetium-99m-MAG3 renal clearance in children: two gamma camera techniques compared with multiple plasma samples. J Nucl Med. 1991;32(9):1704–8.
175. Bailey SM, Evans DW, Fleming HA. Intravenous urography in investigation of hypertension. Lancet. 1975;2(7924):57–8.
176. Chervu LR, Blaufox MD. Renal radiopharmaceuticals–an update. Semin Nucl Med. 1982;12(3): 224–45.
177. Ram MD, Evans K, Chisholm GD. A single injection method for measurement of effective renal plasma flow. Br J Urol. 1968;40(4):425–8.
178. Razzak MA, Botti RE, MacIntyre WJ, Pritchard WH. External monitoring of ^{113}1-hippuran disappearance as a measure for renal blood flow. Int J Appl Radiat Isot. 1967;18(12):825–8.
179. Mackay A, Eadie AS, Cumming AM, Graham AG, Adams FG, Horton PW. Assessment of total and divided renal plasma flow by ^{123}I-hippuran renography. Kidney Int. 1981;19(1):49–57.
180. Heidenreich P, Lauer O, Fendel H, Oberdorfer M, Pabst HW. Determination of total and individual kidney function in children by means of 123-I-hippuran whole body clearance and scintillation camera. Pediatr Radiol. 1981;11(1):17–27.
181. Thompson Jr IM, Boineau FG, Evans BB, Schlegel JU. The renal quantitative scintillation camera study for determination of renal function. J Urol. 1983;129(3):461–5.
182. Tauxe WN, Tobin M, Dubovsky EV, Bueschen AJ, Kontzen F. A macrofunction for computer processing of comprehensive renal function studies. Eur J Nucl Med. 1980;5(2):103–8.
183. Edward Hsiao, Xinhua Cao, Katherine Zukotynski, Laura Drubach, David Zurakowski, Royal T. Davis, Frederic H. Fahey and S. Ted Treves A. Hans Vija, Amos Yahil. Dose reduction in pediatric MAG-3 renal scans J Nucl Med. 2009;50 (Suppl 2): 253.